THESIS

RAMAN STUDIES IN $NH_4H_2PO_4$ AND KH_2PO_4

Submitted by

Theodore Waldo Broberg

In partial fulfillment of the requirements

for the Degree of Doctor of Philosophy

Colorado State University

Fort Collins, Colorado

January, 1972

COLORADO STATE UNIVERSITY

JANUARY, 1972

WE HEREBY RECOMMEND THAT THE THESIS PREPARED UNDER OUR SUPERVISION BY THEODORE WALDO BROBERG ENTITLED RAMAN STUDIES IN $NH_4H_2PO_4$ AND KH_2PO_4 BE ACCEPTED AS FULFILLING IN PART REQUIREMENTS FOR THE DEGREE OF DOCTOR OF PHILOSOPHY.

Committee on Graduate Work

David A. Krueger

Carl H. Liu

J. C. Raich

Ce Giao-yao Yu

Adviser

Ted V. Berlincourt

Head of Department

ABSTRACT OF DISSERTATION

RAMAN STUDIES IN $NH_4H_2PO_4$ AND KH_2PO_4

Laser Raman spectra for $NH_4H_2PO_4$ (ADP) and KH_2PO_4 (KDP) are presented as a function of temperature in the region above the phase transitions. Evidence is presented confirming the existance of strong coupling between the proton B_2 tunneling mode and the B_2 optical phonon mode in both crystals. The spectra were fit to a coupled oscillator function and the relevant fitting parameters are presented. The Debye relaxation time and soft mode frequency for the overdamped mode as well as the static dielectric susceptibility are plotted as a function of temperature. Soft mode behavior in both crystals displays the $\omega^2 \propto (T-T_c')$ dependence. For KDP T_c' was determined to be 30° K. Room temperature spectra are presented for KDP and ADP, and five of the six optical phonon modes are identified. The $(PO_4)^{3-}$ ion modes are observed to split under the local crystalline field of S_4 symmetry and a librational mode of the $(NH_4)^+$ ion is resolved.

Theodore Waldo Broberg
Physics Department
Colorado State University
Fort Collins, Colorado 80521
January, 1972

ACKNOWLEDGMENTS

I wish to express my gratitude to my thesis advisers, Dr. C. Y. She and Dr. David F. Edwards for their help and encouragement during this research. I also want to thank my committee for their help and cooperation. Clinton Meneely, Elwood Schapansky and Larry Wall are to be thanked for helpful discussions. I am especially grateful to my wife and three children, who have provided much encouragement and have displayed remarkable faith and understanding during my graduate work.

TABLE OF CONTENTS

LIST OF TABLES

LIST OF FIGURES

CHAPTER I

THE NATURE OF THIS RESEARCH

Materials displaying ferroelectric properties have captured the interests of many researchers in recent years. This interest has stimulated many theoretical and experimental studies of the phase transition in these materials which has resulted in a qualitative understanding of the mechanisms involved. The classification of ferroelectrics into displacive type and order-disorder type has been fruitful.[1] The soft-mode which describes the transition of the displacive ferroelectrics[2] beautifully, is usually broad and in many cases unobserved in the order-disorder ferroelectrics. This makes the interpretation of the dynamics of the order-disorder ferroelectric transition difficult and often speculative.

The dynamics of the phase transition in crystal potassium dihydrogen phosphate (KH_2PO_4 or KDP) and ammonium dihydrogen phosphate ($NH_4H_2PO_4$ or ADP) has long been speculated[3] in terms of the tunneling motion of the hydrogen ions in a double-well potential which achieves ferroelectric order for KDP and anti-ferroelectric order in ADP below the transition temperature. That this picture is qualitatively correct is supported by neutron diffraction studies which show the proton charge distribution between two oxygen ions

perpendicular to the crystal c-axis to be symmetric and asymmetric, respectively, above and below the phase transition temperature. Among others, Blinc[4], deGennes[5], and Tokunaga[6] have worked out the thermodynamics of this type of ferroelectric phase transition (KDP) using a quasi-spin formalism. Their results are in qualitative agreement with dielectric constant measurements.[7] No attention was paid directly to the anti-ferroelectric transition in ADP.

The quasi-spin tunneling picture of KDP had many weaknesses. It could not account for the insensitivity of the spontaneous polarization to deuteration, nor could it explain what would cause the spontaneous polarization in KDP, which is parallel to the c-crystallographic axis, to be perpendicular to the proton tunneling motion. A major step in the right direction was taken as Kaminow, et. al.[8] reported the softening of the broad low-frequency wing in the B_2 (Raman) spectrum of KDP when the temperature is lowered towards the phase transition, and Kobayashi[9] proposed the coupling of an optical phonon and the proton tunneling mode which causes the displacements of potassium and phosphate ions along the c-axis to "freeze in" below the transition temperature. Thus, there was qualitative understanding of the problem when this research began. The ferroelectric phase transition of KDP was triggered by the long range ordering of the proton tunneling motion which causes a spontaneous polarization along the c-axis through the proton-phonon coupling.

Several questions in need of answers arose naturally at the beginning of this research. Some of these, of course, were spawned in the light of preliminary studies by us as well as research by others. Some of our early questions can be summarized as follows:

There are four tunneling protons in a primitive cell of the high temperature phosphates (KDP and ADP); they may be decomposed[10] into $A_2 + B_2 + E$ modes under the crystal point group D_{2d}. The A_2 mode is Raman inactive, but one would like to follow the dynamical behavior of the E mode as well as the B_2 mode in KDP. Can one observe the broad fluctuations (B_2 and E) in ADP? Furthermore, the effect of the proton-phonon coupling should be studied experimentally. What are the effects of this coupling on the temperature dependent polarization fluctuations, and thus on the dynamics of the phase transition? Also, our preliminary spectra revealed many line shape anomalies at room temperature. Can one obtain information on the order parameter by following the temperature dependence of some of the line shape anomalies? Finally, can all or most of the Raman active modes in ADP and KDP be identified?

To answer these questions, two efforts were planned for this research: (1) room temperature Raman spectroscopy of KDP and ADP in an attempt to identify Raman lines and to note the significance of the line-shape anomalies, and (2) temperature dependent B_2 and E Raman spectra of KDP and ADP below 300 cm^{-1} in an attempt to

follow the dynamics of the tunneling modes and the effect of the proton-optical phonon coupling.

Due to the efforts of this research and the independent efforts of several other groups during 1971, most of these questions are answered, at least qualitatively. This thesis will present data and their interpretations conducted in this laboratory. Whenever possible, a comparison with recent publications and intended publications (preprints) will be given. All of the experiments presented here were planned in the beginning of this project and they were performed at Colorado State University without the prior knowledge of the work of others.

It should be pointed out that even if all the questions raised here were answered, our understanding of ferroelectrics would still be rudimentary. Compared to magnetic transitions, there exists no well-established Hamiltonian and no discussion of ferroelectrics beyond the mean-field theory. The whole question of the microscopic interactions and critical exponents is unexplored in ferroelectric and anti-ferroelectric materials.

CHAPTER II

THE OPTICAL PHONONS OF TETRAGONAL KH_2PO_4 AND $NH_4H_2PO_4$

In general all of the vibrational modes in a crystal are not Raman active (capable of giving rise to a Raman shift). It is therefore necessary in the course of a Raman analysis to predict which of the vibrational modes of the sample are Raman active. Fortunately there are well established procedures for doing this based upon group theoretical results.[11] These procedures allow the decomposition of a system of atoms into its normal modes of vibration. It is then possible to determine whether a mode is Raman active from its transformational properties.

The symmetry of the crystal KDP and ADP at room temperature is represented by the space group D_{2d}^{12}. The point group of the unit cell is D_{2d}. It is the point group which is of interest in this study since it portrays the symmetry of the long wave lattice modes and the center of the Brillouin zone. Only the long wave (k=0) phonons can be detected in the first-order Raman scattering due to the conservation of wave vectors, and the symmetry of the center of the Brillouin zone is therefore of paramount importance to Raman scattering.

The high-temperature phase of the KDP (or ADP) crystal is tetragonal. It may be regarded as consisting of K^+ (or NH_4^+) and $(H_2PO_4)^-$ ions with two K^+ (or NH_4^+) ions and two $(H_2PO_4)^-$ ions in a primitive cell. The unit cell of this structure is shown in Figure 1 and more detail of the crystal structures of KDP and ADP in both low and high temperature phases are presented in Appendix I.

In view of this crystal structure, it is natural to divide the vibrations of tetragonal KDP (or ADP) into lattice modes describing the relative motions of K^+ (or NH_4^+) and $(H_2PO_4)^-$ ions, internal modes and librational modes of PO_4^{3-} and NH_4^+ ions, and the vibrations related to the tunneling motion of the protons in the $(H_2PO_4)^-$ ions. The correlation method[11] may be applied to decompose these degrees of freedom into the irreducible representations of the point group of the crystal D_{2d}. The procedures for doing this can be found in the literature[12] and will not be repeated here.

In a recent publication[13] we analyzed the KDP crystal in terms of the lattice modes and the $(PO_4)^{3-}$ internal modes. The symmetry of our spectra demonstrated that the $(PO_4)^{3-}$ ion remains as an essentially individual structure in the crystal and its Raman active modes are split by the local crystalline field. A more detailed analysis of this $(PO_4)^{3-}$ mode splitting is presented by G. L. Paul and H. Montgomery.[14] Further independent experimental results are reported by Coignac and Poulet.[15]

Figure 1. Unit cell (not primitive) of KDP, ADP. Numbers (1, 2, 3, 4) denote inequivalent sites in the primitive unit cell. Unit cell dimensions: KDP ($a = 7.448$ Å, $c = 6.977$ Å @ 299 °K), ADP ($a = 7.510$ Å, $c = 7.564$ Å @ 247 °K).

O : K^+, NH_4^+

● : $(H_2PO_4)^-$

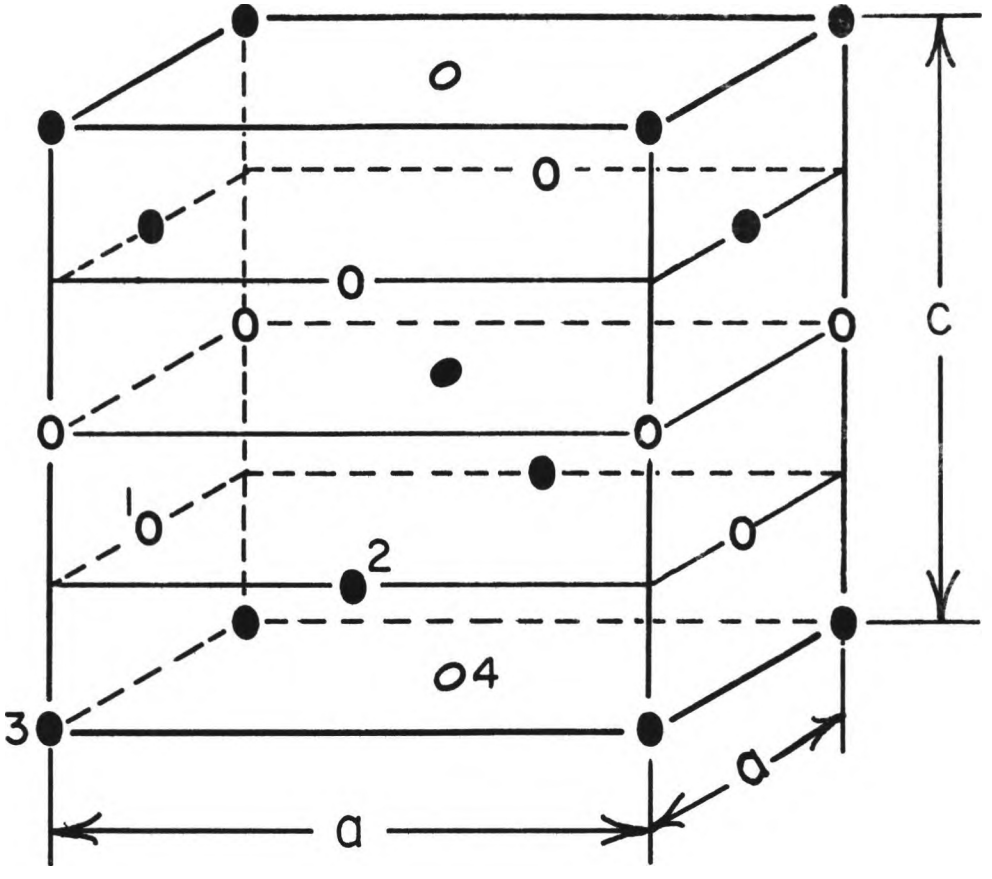

The remainder of this chapter will be devoted to presenting the room temperature Raman data for the ADP and KDP crystals.

Lattice Modes of the KDP and ADP

The Raman spectra of ADP and KDP up to a 700 cm^{-1} shift were taken with a He-Ne laser used for excitation at room temperature (294°K). The spectra of KDP have been reported by us.[13] A slight misalignment of the crystal used in that publication caused some leak through from modes of undesired species. An improved alignment of the crystal used for the data in Figure 3 eliminates this leak through and results in a cleaner spectrum.

The room temperature ADP data below 700 cm^{-1} are presented in Figure 2. The notation used for the incident and scattered light is standard. For example, y(xy)x indicates that the incident light travels along the y crystallographic direction, polarized in the x direction, the scattered light goes out x polarized in the y direction.

The optical lattice modes lie below 300 cm^{-1}. Popova and Stekanov[16] were able to identify three of the six optical lattice modes predicted by group theory in KDP. They did not analyze both the incident and scattered polarization, however, and therefore were unable to isolate the contributions to the Raman spectrum of the other optical lattice modes. Group theory[13] decomposes the lattice modes into B_2+E acoustic phonons and $2B_1+B_2+E$ optical phonons. In this research, five of the six optical modes predicted by group theory

Figure 2a. Room temperature Raman spectra of ADP below 700 cm^{-1}. The ordinate is calibrated in scattered photon counts. Notation is as follows: y(zz)x and y'(x'y')x' refer to the A_1 and B_1 species respectively. Resolution is 4 cm^{-1} at 6, 328 Å.

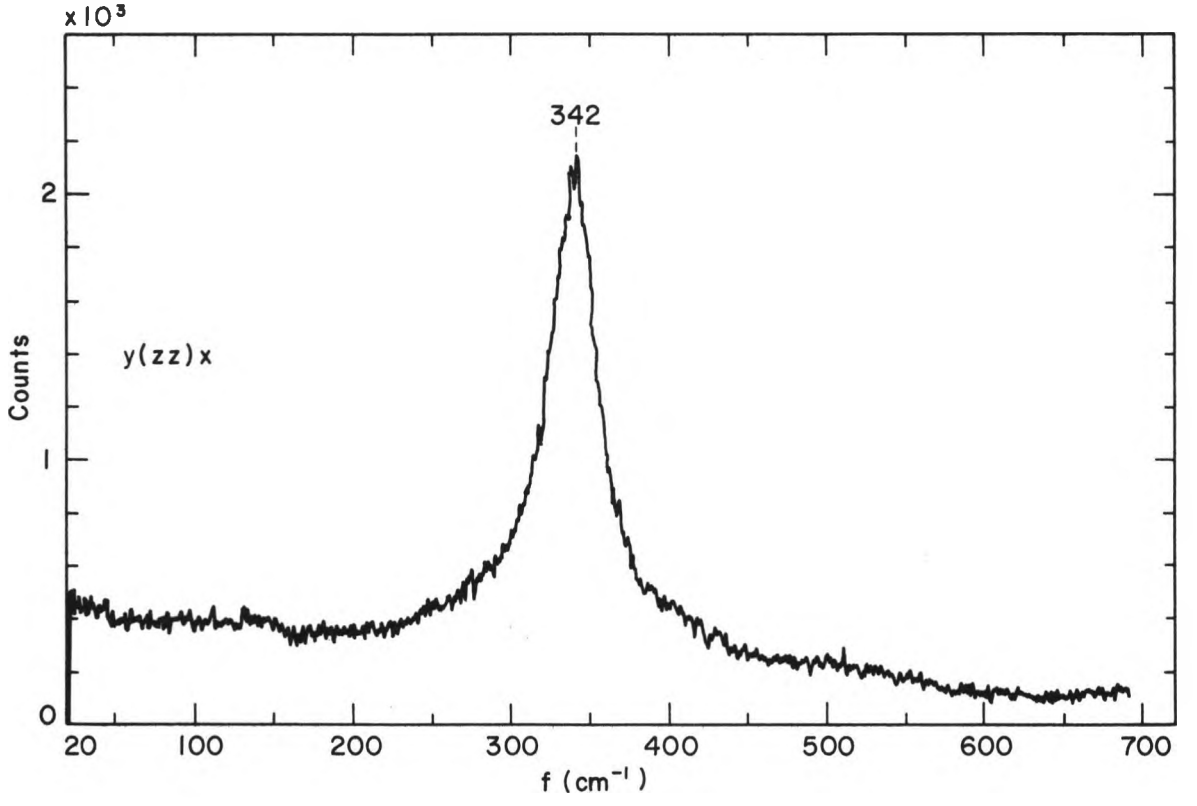
x10³
342
2
1
0
Counts
y(zz)x
20
100
200
300
400
500
600
700
f (cm⁻¹)

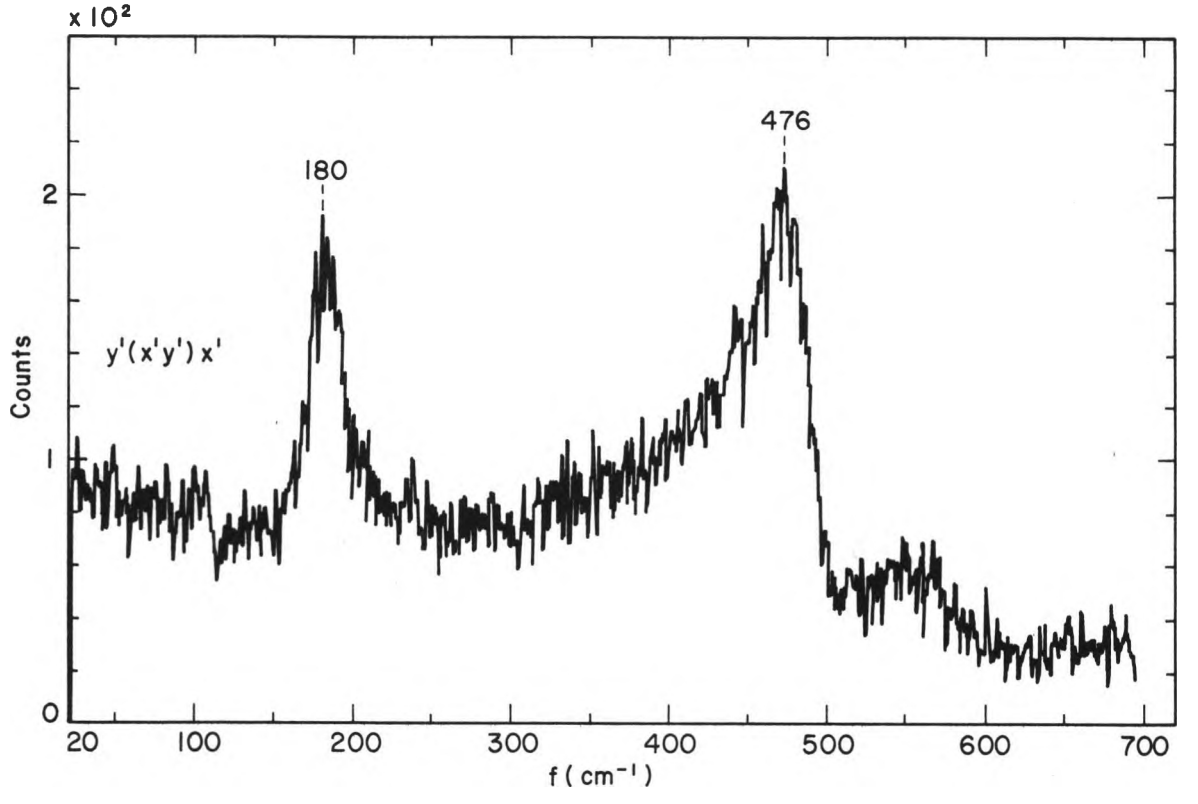
x10²
476
180
2
1
0
Counts
y'(x'y')x'
20
100
200
300
400
500
600
700
f (cm⁻¹)

Figure 2b. Room temperature Raman spectra of ADP below 700 cm^{-1}. The ordinate is calibrated in scattered photon counts. Notation is as follows: y(xy)x and y(xz)x refer to the B_2 and E species respectively. Resolution is 4 cm^{-1} at 6, 328 Å.

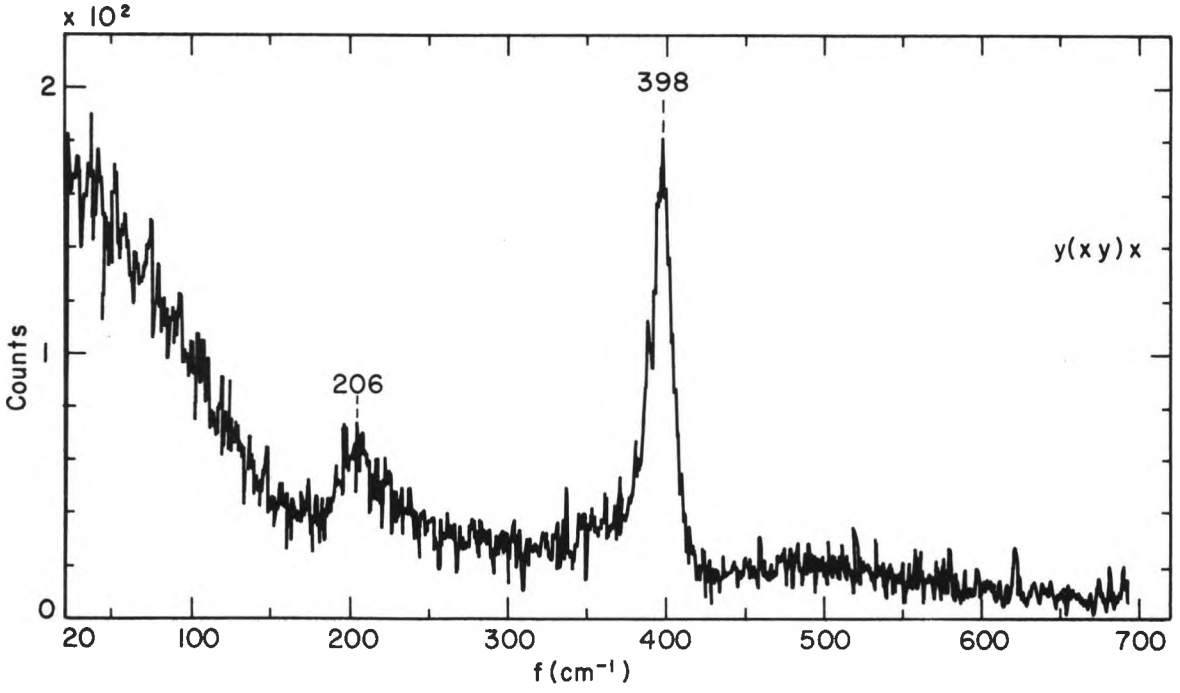
x 10²
2
1
0
Counts
398
206
y(x y) x
20
100
200
300
400
500
600
700
f(cm⁻¹)

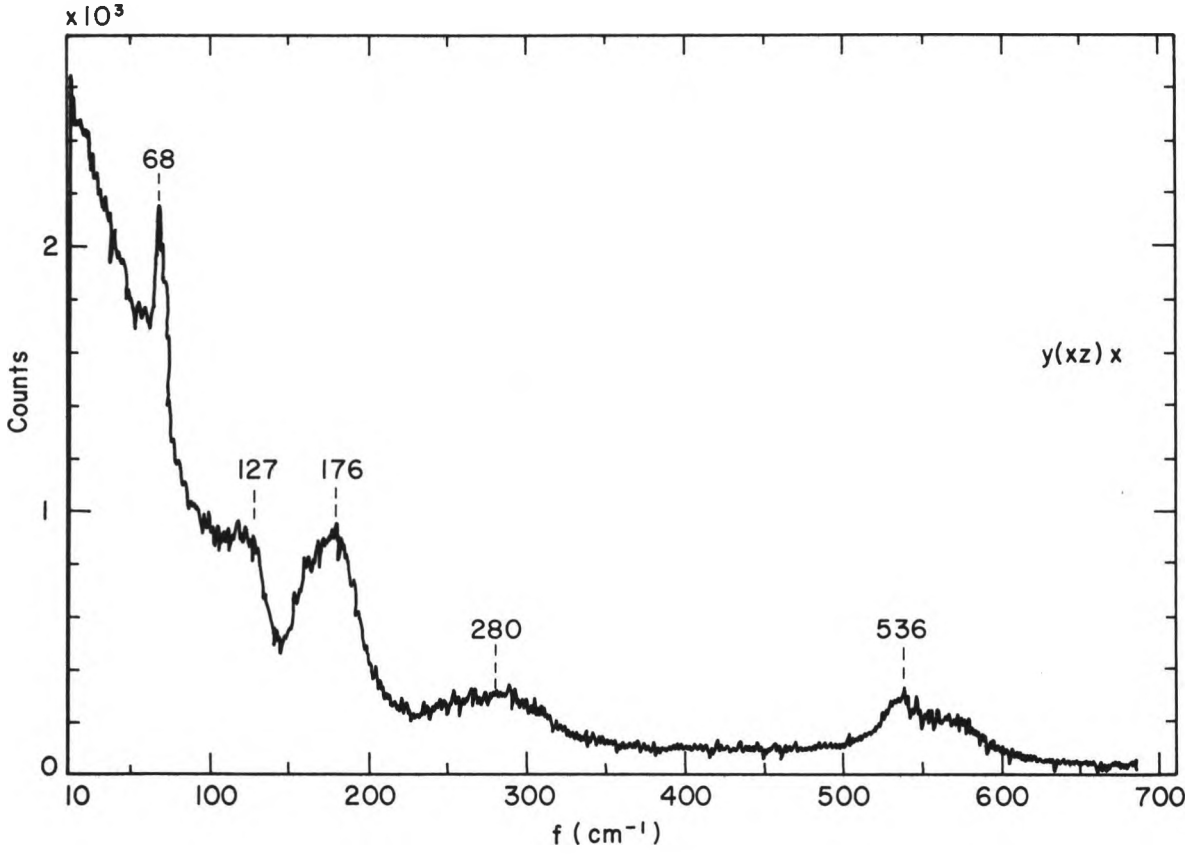
x10³
2
1
0
Counts
68
127
176
280
536
y(xz) x
10
100
200
300
400
500
600
700
f (cm⁻¹)

were unambiguously identified. The positions and full widths at half maximum of the lattice modes for both KDP and ADP are included in Table 1. Success in identifying these modes can be attributed to the improvement of our signal-to-noise ratio and to a judicious choice of sample orientation for the B_1 spectrum. A good signal-to-noise ratio allowed the luxury of analyzing the polarization of both the incident and scattered light. This made a positive identification of a mode of α_{ij} symmetry possible. The sample used for all spectra except B_1 was a rectangular solid with the faces oriented perpendicular to the crystallographic x, y and z directions. This orientation allowed unambiguous identification of modes of the A_1, B_2 and E species. The B_1 spectrum was observed using a sample which was different from the other only in that the faces perpendicular to the z faces were rotated from the x, y directions by 45°. These new faces are referred to here as x', y' faces. This sample orientation allowed the B_1 modes to be distinguished from the A_1 modes.

The acoustic phonons are not observable in a Raman experiment because their frequency shifts are smaller than the resolution of the Raman spectrometer system. Two optical lattice modes of B_1 symmetry were predicted by group theory but only one was found. The other line was not found in searches down to 4 cm^{-1} shift. There is in ADP a depression in the B_1 spectrum near 110 cm^{-1}. This interesting feature can be seen more clearly when an argon laser is used as an excitation source and this is shown in Figure 3b. It is not impossible that the weak B_1 mode is near this location and what one sees in

Table 1. Line parameters for the Raman active lattice modes in ADP and KDP at 294° K. Resolution at the exciting wavelength is 4 cm^{-1}.

Symmetry Species	ADP		KDP	
	Position (cm^{-1})	FWHM (cm^{-1})	Position (cm^{-1})	FWHM (cm^{-1})
B_1	180	18	151	10
B_2	206	41	180	27
E	68	8	96	9
	127	15	114	7
	176	37	190	21

Figure 3b is the interference spectrum of the two lattice B_1 modes in ADP. A temperature dependent study of this structure was made and the structure remains essentially temperature independent between 146° K and 294° K.

Internal Modes of $(PO_4)^{3-}$

The free tetrahedral $(PO_4)^{3-}$ ion has four vibrational modes[17] which are Raman active. These consist of an A_1 mode at 980 cm^{-1}, and E mode at 363 cm^{-1} and two F_2 modes at 515 and 1082 cm^{-1}. In crystalline ADP the local crystalline field causes the E vibrations at 363 cm^{-1} and the F_2 vibration at 515 cm^{-1} to split into A+B (at 324 and 398 cm^{-1}) and the B+E (at 476 and 536 cm^{-1}) vibrational modes of S_4 symmetry, respectively. These modes can be seen in Figure 2. The A_1 mode at 980 cm^{-1} can be seen in the y'(zz)x' spectrum and the 1080 cm^{-1} F_2 mode in the y'(x'y')x' spectrum of Figure 3.

The splitting of the $(PO_4)^{3-}$ vibrational modes in KDP follows a very similar format to that in ADP. We previously showed,[13] using symmetry arguments, that the $(PO_4)^{3-}$ ion in the KDP crystal maintains most of its free-ion vibrational characteristics. These vibrations, are split by the local crystalline field as mentioned above.

For the sake of completeness, it should be mentioned that the two inequivalent $(PO_3)^{3-}$ sites per primitive unit cell might be expected to impart different splitting to the $(PO_4)^{3-}$ modes. We did not look carefully for this in our spectra, however. Therefore, the

Figure 3a. ADP Raman Spectra between 50 cm^{-1} and 3500 cm^{-1}. Resolution is 4 cm^{-1} at 4, 880 Å.

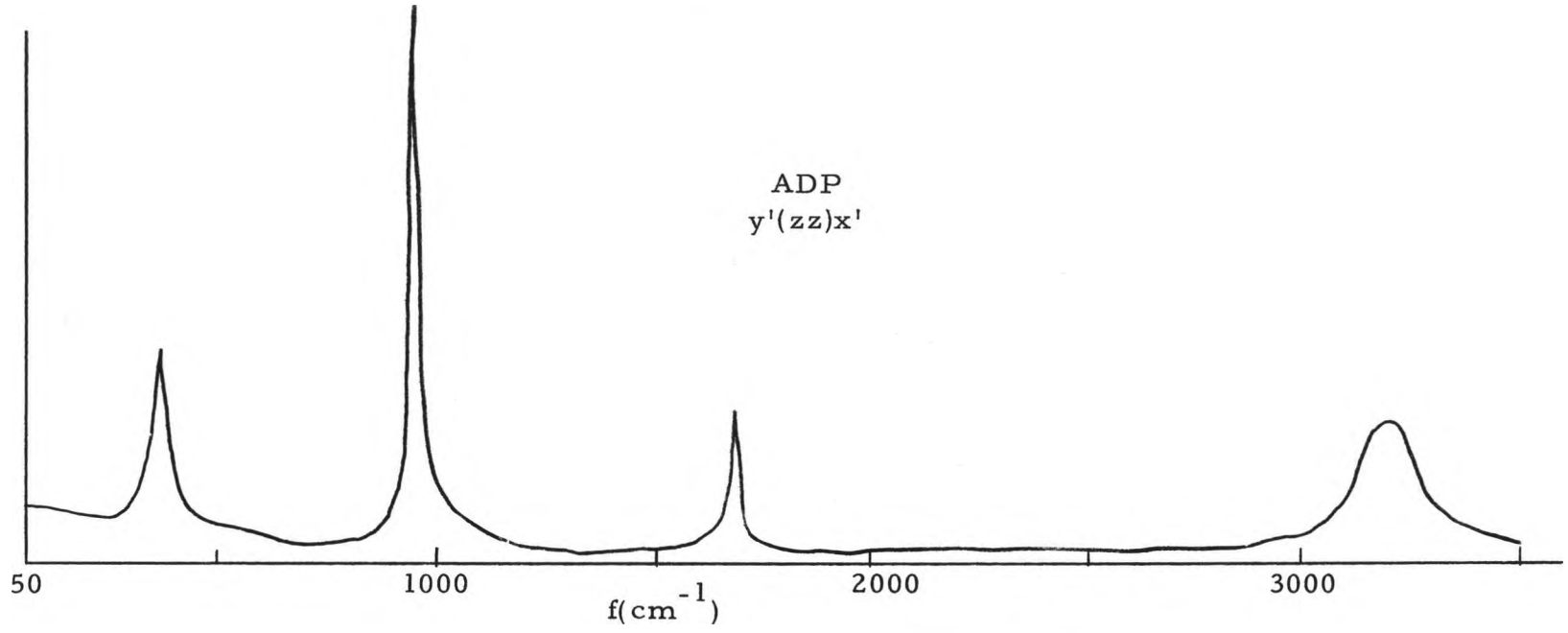
ADP
y'(zz)x'
50
1000
2000
3000
f(cm-1)

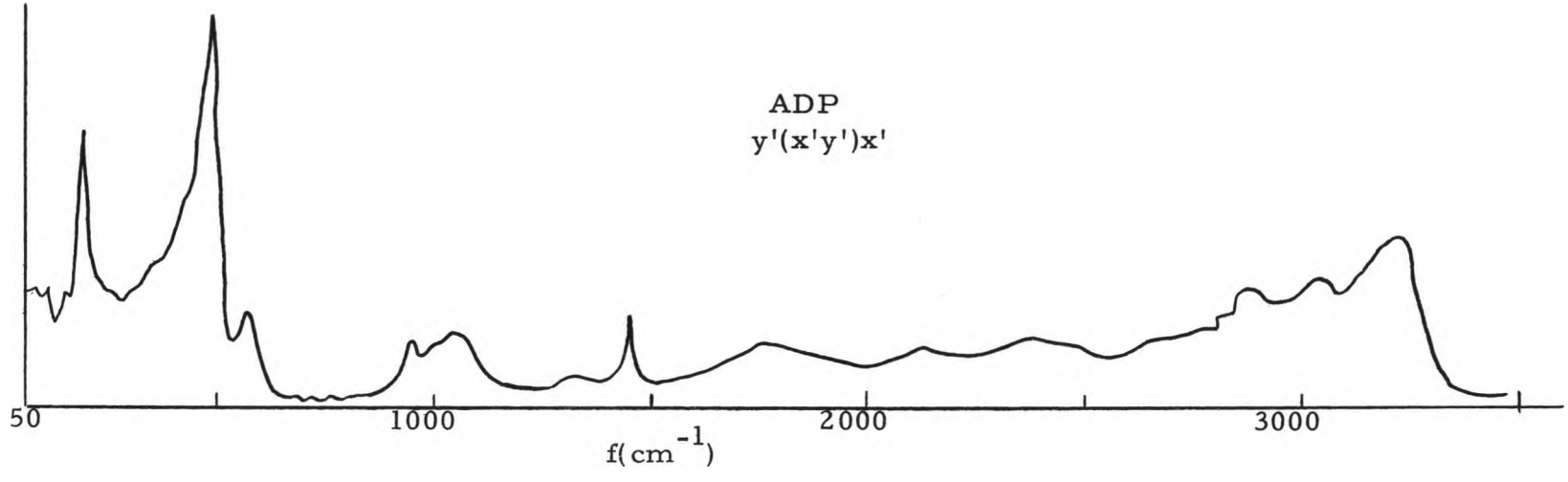
ADP
y'(x'y')x'
50
1000
2000
3000
f(cm-1)

Figure 3b. ADP and Raman Spectra between 50 cm^{-1} and 3500 cm^{-1}. Resolution is 4 cm^{-1} at 4880 Å. Vertical scale change is indicated by dashed line.

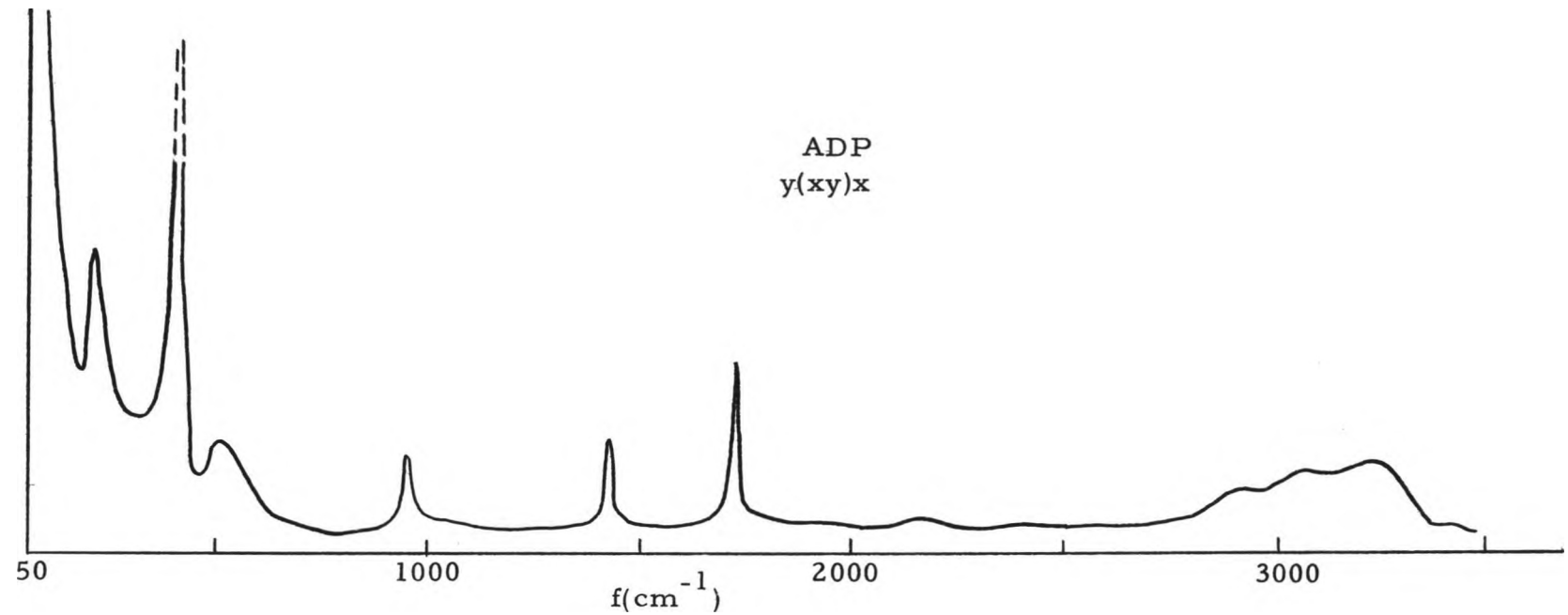
ADP
y(xy)x
50
1000
2000
3000
f(cm-1)

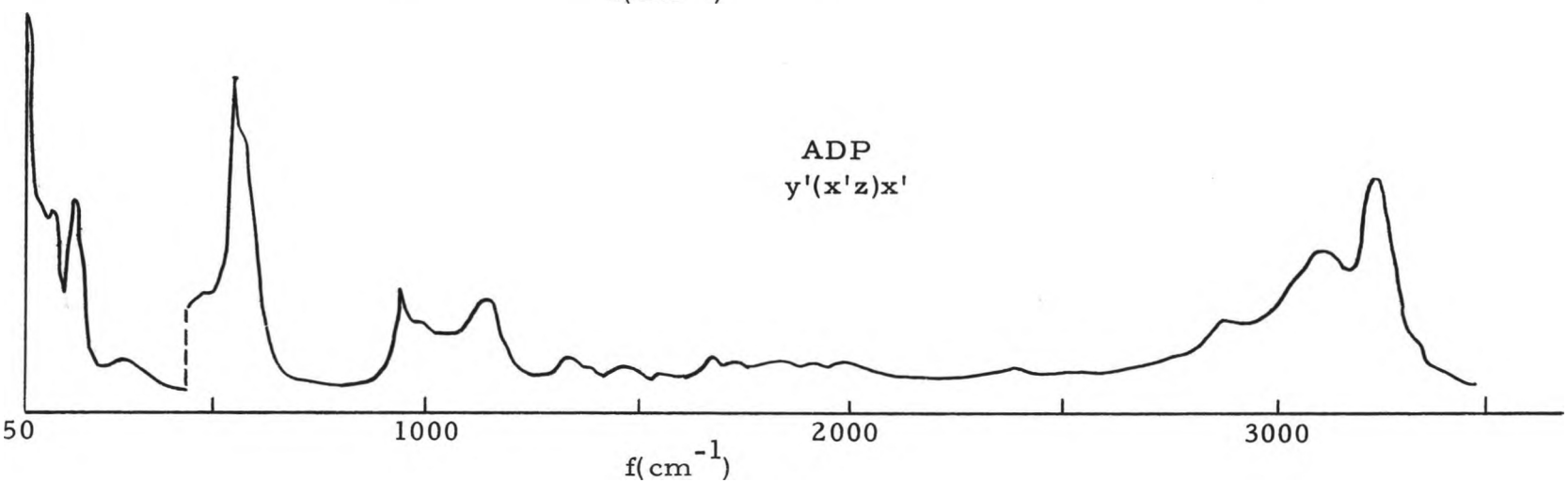
ADP
y'(x'z)x'
50
1000
2000
3000
f(cm-1)

Figure 3c. KDP Raman Spectra between 50 cm^{-1} and 3500 cm^{-1}. Resolution is 4 cm^{-1} at 4880 Å. Vertical scale change is indicated by dashed line.

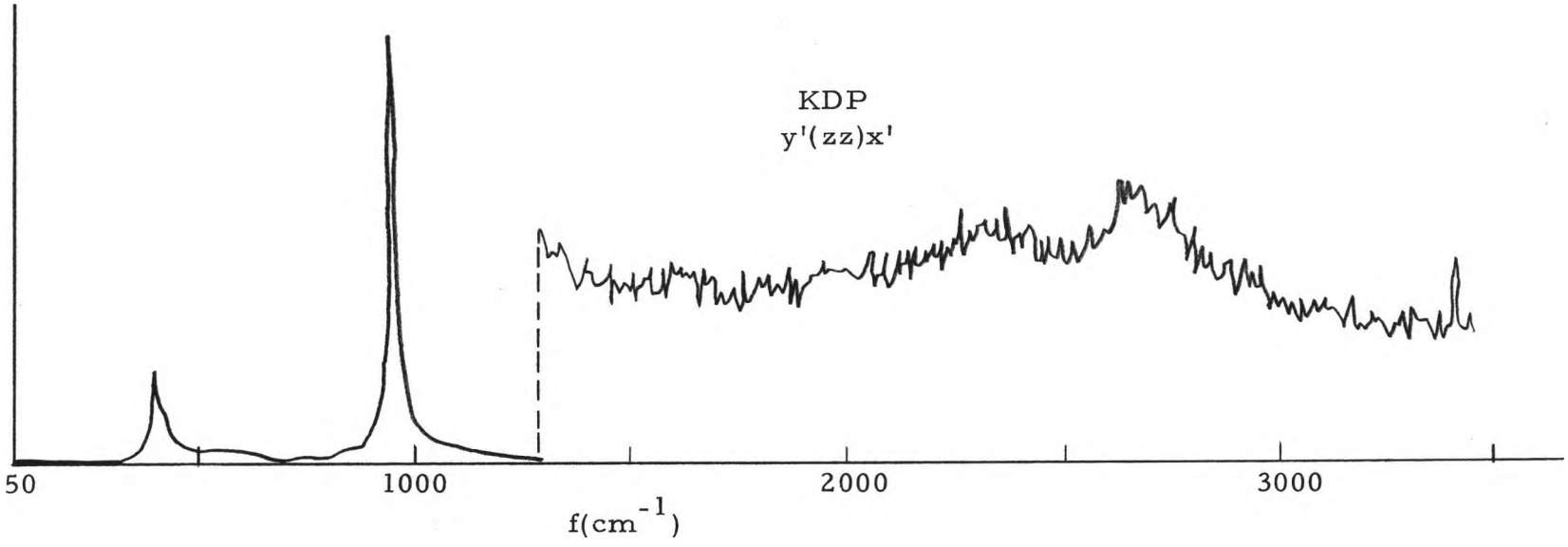
KDP
y'(zz)x'
50
1000
2000
3000
f(cm-1)

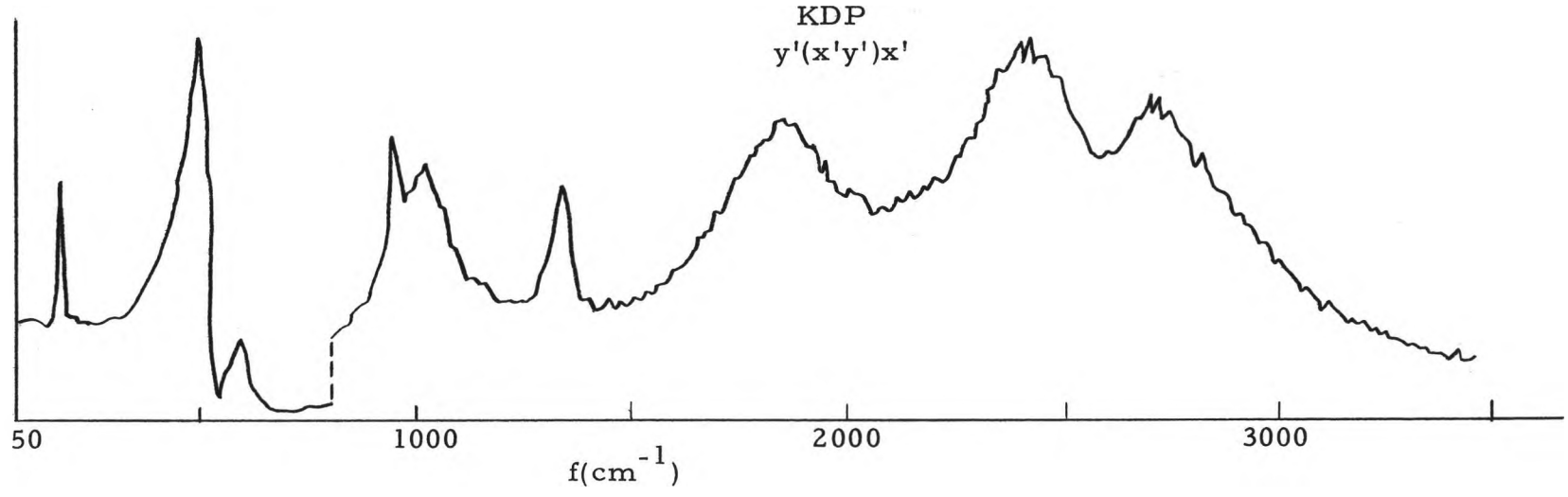
KDP
y'(x'y')x'
50
1000
2000
3000
f(cm-1)

Figure 3d. KDP Raman Spectra between 50 cm^{-1} and 3500 cm^{-1}. Resolution if 4 cm^{-1} at 4880 Å. Vertical scale change is indicated by dashed line.

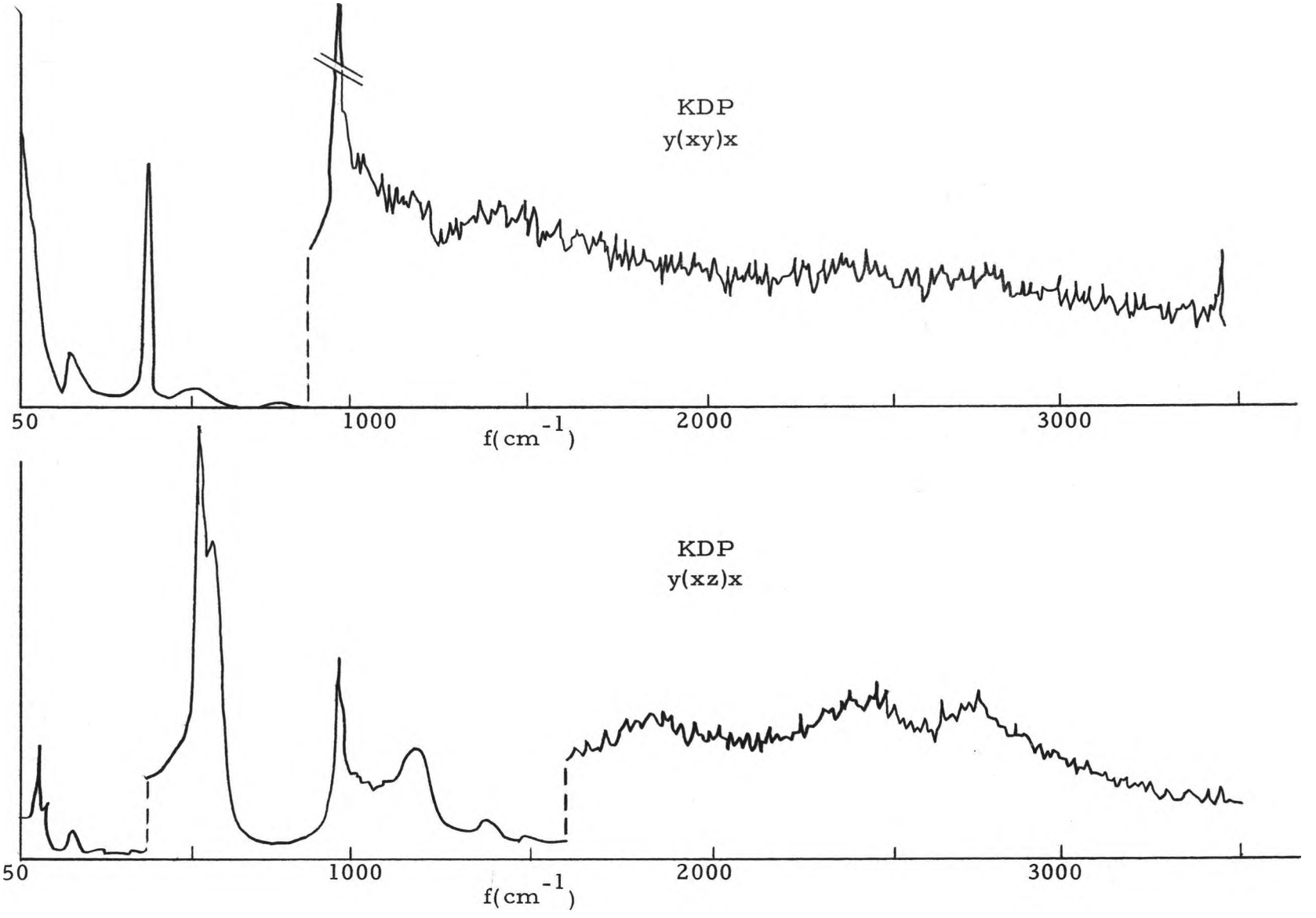
KDP
y(xy)x
50
1000
2000
3000
f(cm-1)
KDP
y(xz)x
50
1000
2000
3000
f(cm-1)

splitting at the two sites is assumed to be equivalent to within the resolution of our experiment.

Internal Modes of $(NH_4)^+$

The E y(xz)x spectrum of Figure 2 reveals a broad mode at about 280 cm^{-1}. This line can be identified as an E librational (torsional) mode of the $(NH_4)^+$ complex in the ADP lattice. This classification is possible because the F_1 rotational modes of $(NH_4)^+$ of symmetry T_d correlate into the A_2 + E species of D_{2d} symmetry. Also the 280 cm^{-1} location is in agreement with librational frequency ranges in other ammonium salts.[18]

Evidence of the other vibrational modes of the $(NH_4)^+$ ion can be found in the frequency region above 1000 cm^{-1} in Figure 3. The structure in this region of our spectra is in part due to oxygen-hydrogen vibrations and agrees well with infrared spectra published by others.[19]

Hydrogen Tunneling Modes

The orientation of the hydrogen bonds in ADP and KDP is discussed in detail in Appendix I. The hydrogens move in double-well potentials and above the phase transition temperature tunnel from one well to the other. The hydrogen motion[10] is almost entirely parallel to the bond direction and represents four degrees of freedom due to the four hydrogens per primitive unit cell. Therefore there are

Figure 4. Schematic representation of the four proton tunneling modes in KDP and ADP.

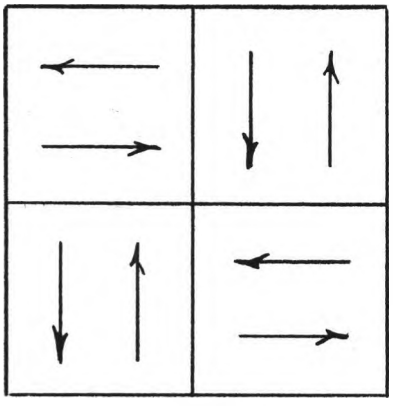

A_2

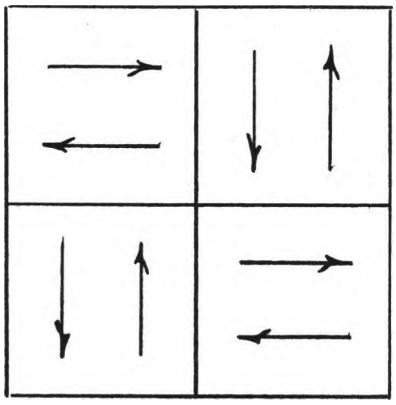

B_2

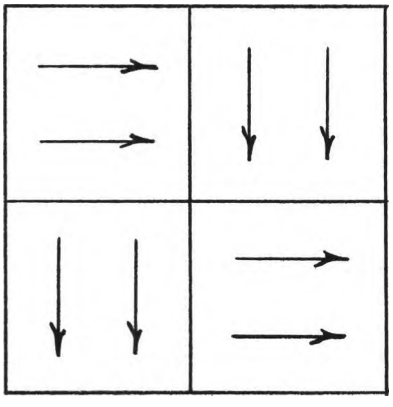

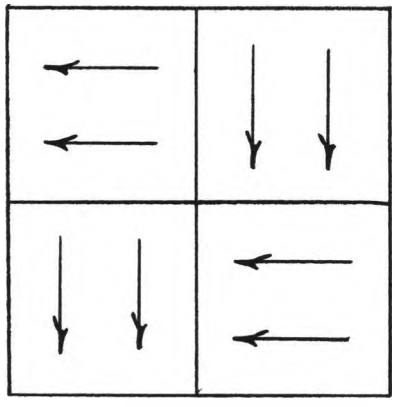

E

four one dimensional modes (represented schematically in Figure 4) which transform according to the irreducible representation of D_{2d}. The hydrogen motion can be decomposed into the $A_2 + B_2 + E$ species of D_{2d}. The A_2 mode is Raman inactive but the B_2 and E modes can couple to lattice modes of the same species. Evidence of this coupling is seen in the low energy wings of the ADP and KDP room temperature spectra of Figure 5. These modes are associated with the polarization fluctuations in the crystal to be discussed in the next chapter.

The gross wing-like features of the y(xy)x and the y(xz)x spectra of Figure 2 below about 150 cm^{-1} for ADP are very similar in shape and transform as the electric polarizations P_z and P_x(and/or P_y), respectively. Kaminow and Damen[8] first reported a similar structure in the y(xy)x spectrum of KDP as being due to polarization fluctuations characteristic of ferroelectricity (i. e., the ferroelectric mode). Analogously, we attribute the low energy wings of Figure 2 to polarization fluctuations associated with antiferroelectricity in ADP. The general shape of the low energy wings of the B_2 and E spectra of ADP are seen to be quite similar. In KDP, however, the wings in the B_2 and E modes are quite dissimilar. This difference between the ADP and KDP spectra is probably due to the fact that the anisotropy in ADP due to the antiferroelectric mode has a "spatial period" about the size of the unit cell. To the 4880A light ADP would appear quite isotropic insofar as the polarization is concerned. The ferroelectric mode in KDP at $k = 0$ on the other hand produces a long wave

Figure 5. y(xy)x and y(xz)x spectra below 300 cm^{-1} for ADP and KDP. Numbers on vertical scale are photon counts and on the horizontal scale are cm^{-1}. The factor of 6.7 multiplying the scale of the y(xy)x spectrum of ADP compensates for the polarization dependence in the spectrometer transmission.

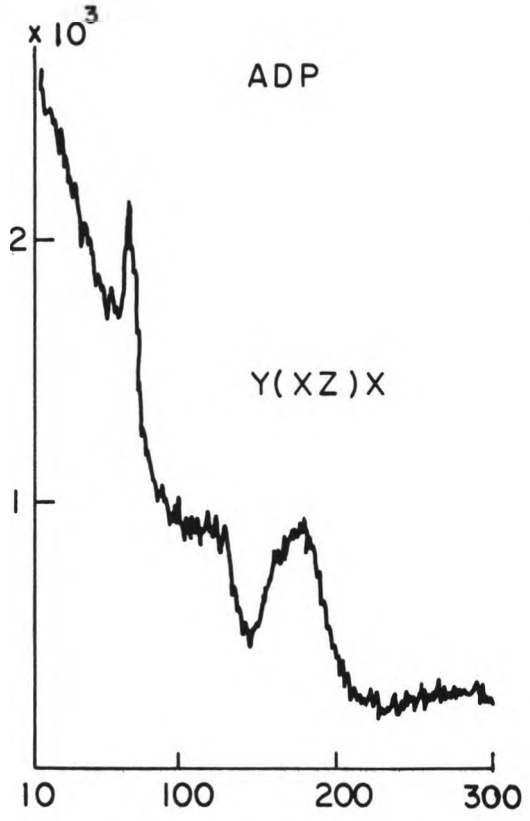
x 10³
ADP
Y(XZ)X
2
1
10
100
200
300

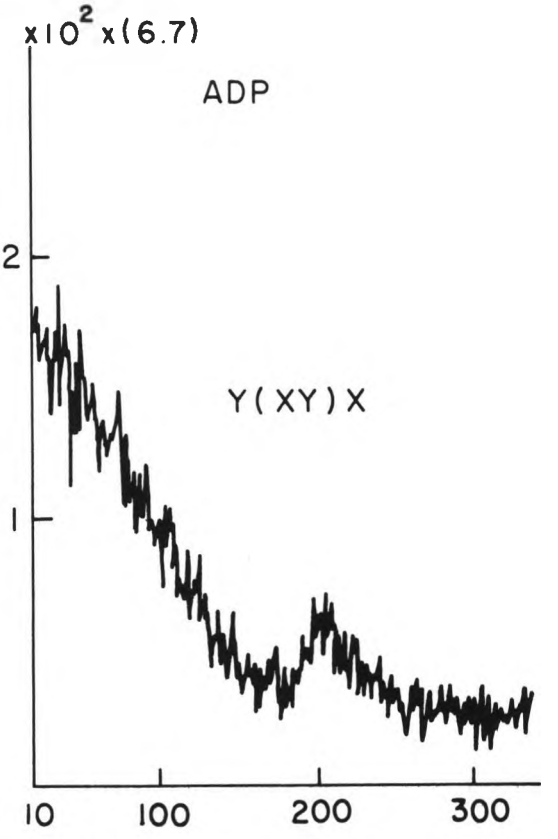
x10² x(6.7)
ADP
Y(XY)X
2
1
10
100
200
300

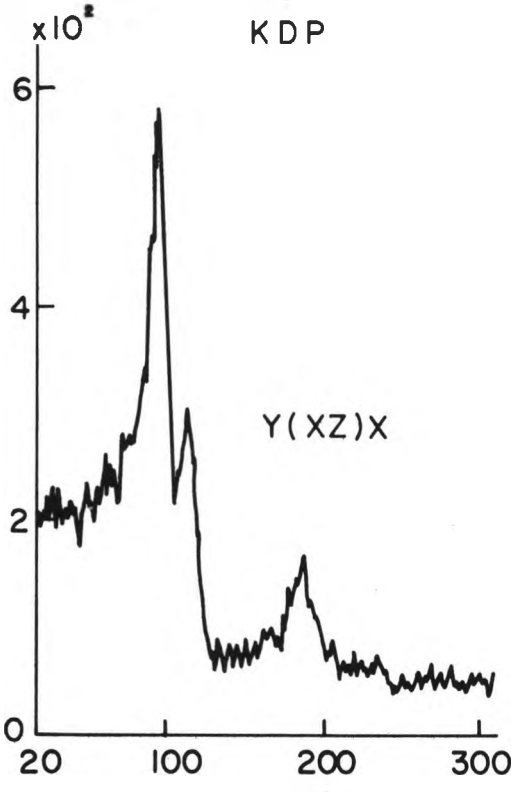
x10²
KDP
Y(XZ)X
6
4
2
0
20
100
200
300

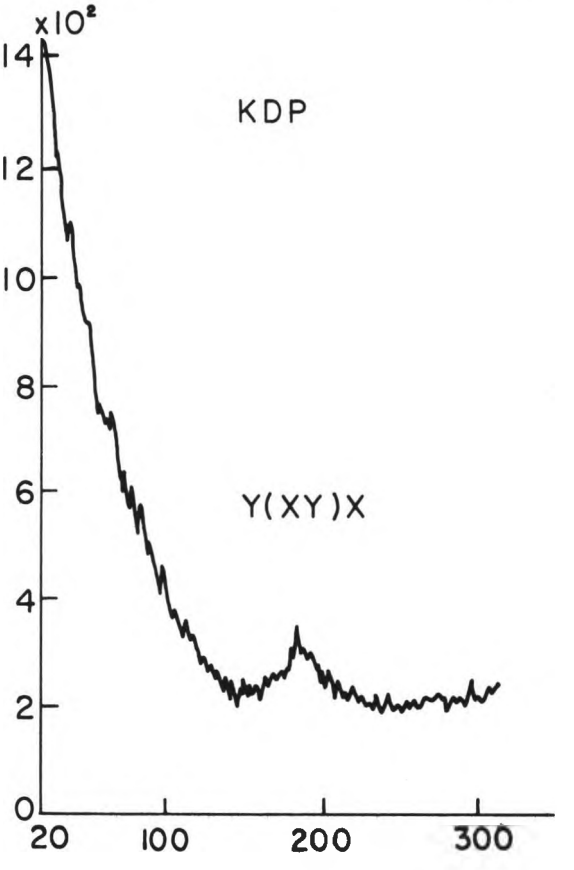
x10²
KDP
Y(XY)X
14
12
10
8
6
4
2
0
20
100
200
300

anisotropy in the crystal for which our 4880 A light is an ideal probe. Hence in KDP, Raman scattering is sensitive to the anisotropy whereas in ADP it is not.

CHAPTER III

TEMPERATURE DEPENDENT POLARIZATION FLUCTUATIONS IN $NH_4H_2PO_4$ AND KH_2PO_4

The paralelectric to ferroelectric phase transition which occurs in KDP at about 122°K has been a subject of interest for many years. During this time the mechanism responsible for the transition has remained a matter of speculation. It is well established that the four hydrogen ions in the primitive cell play an important role in the phase transition mechanism.[9] This information is based partially on the very large hydrogen isotope effect on the transition temperature T_c. KH_2PO_4 undergoes its phase transition at 122°K while deuterated KDP (KD_2PO_4) has its phase transition at 213°K. Neutron diffraction studies had revealed that the hydrogen motion in the lattice was almost exclusively along its bond axis which in turn is virtually perpendicular to the c-axis of the KDP crystal. Other studies revealed that there was no appreciable isotope effect in the saturated dielectric polarization. X-ray diffraction data[20] have shown that in the ferroelectric phase K^+, P^{5+} and O^{2-} ions are displaced parallel to the c-axis relative to their symmetric positions in the paraelectric phase. These displacements have been shown to adequately account for the observed magnitude of the saturated polarization. It was, therefore, apparent that this hydrogen motion could not directly account for the ferroelectric polarization along the c-axis of the crystal.

Nevertheless, de Gennes,[5] Blinc[4] and others devised a pseudo-spin model for the tunneling motion of the hydrogen ions in a double well potential. The large isotope effect on the transition temperature could be accounted for with this model because of the dependence of the tunneling frequency on the mass of the hydrogen ion. However, the model could not account for the polarization being perpendicular to the hydrogen motion, or for the lack of isotope effect on the saturated polarization.

In 1968, Kobayashi[9] proposed a theory which admitted a coupling between the hydrogen tunneling mode and an optical phonon mode involving the motion of the K^{+}, P^{5+} and O^{2-} parallel to the crystallographic c-axis. This is to say, the proton position in the double well could be directly related to the positions of the K^{+}, P^{5+}, O^{2-} ions in the ferroelectric phase. As the hydrogens in a region of the crystal tunneled between the two wells, the polarization of the crystal could flip between its two possible directions along the c-axis. Thus the frequency of one of the coupled modes could tend to zero, or become soft, as the curie temperature is approached from above due to the"collective ordering"of the hydrogens at this temperature.

In 1968 Kaminow and Damen[8] reported making the first observation of an overdamped soft mode in the B_2 spectrum of KDP by Raman scattering. More recently, Wilson and Cummins[21,22] did

a similar but more detailed Raman study of this mode. Ryan[23], et.al., have included the coupling of the over damped B_2 mode with the closest B_2 optical mode in KDP and ADP at room temperature. The asymmetry in these lines suggests that the coupling should be considered. The KDP work of Ryan, et.al., was only at room temperature and the only parameter they report is the relaxation time for the over damped mode. They also report the temperature dependence of the Debye relaxation time for both the B_2 and E modes in ADP.

The research presented in this section, independently, represents an investigation of the overdamped modes in ADP and KDP. Temperature dependent experimental spectra of the B_2 and E modes below 300 cm^{-1} in both ADP and KDP were taken. Their dynamic behaviors are probed from both above and below the phase transition in KDP and only from above in ADP. Results are analyzed only for the B_2 modes in both ADP and KDP for temperatures approaching the transition from above. The spectra are fit to a two coupled-mode harmonic oscillator function using a least squares fitting program.[24] This is the first time that the coupled mode problem in KDP has been studied as a function of temperature. The B_2 study for ADP copes with the optical mode coupling as a function of temperature as does the work of Ryan, et.al., but our more complete data and precision in temperature control allows a much improved analysis.

Spectral Analysis

The coupled proton-optical-phonon modes of the crystal are Raman active as well as infrared active. It is therefore possible to observe this mode coupled to the proton tunneling system using Raman spectroscopy. The power spectrum $Q(\omega)$ of the fluctuations in q is related to the imaginary or dissipative part of the dielectric susceptibility through the fluctuation-dissipation theorem.[25,33] The Raman spectrum for Stokes transitions is then given by (Appendix II)

$$F_{ij}(\omega) = A' \left| \frac{\partial \alpha_{ij}}{\partial q_k} \right|^2 Q(\omega)$$

$$= A' \left[n(\omega) + 1 \right] \left| \frac{\partial \alpha_{ij}}{\partial q_k} \right| \chi''(\omega)$$

where α_{ij} is an element of the electronic polarizability tensor, z is an effective charge, q_k is a normal mode coordinate, $\chi''(\omega)$ is the imaginary part of the dielectric susceptibility and $n(\omega) = (\exp\frac{\hbar\omega}{kT} - 1)^{-1}$ is the Bose factor. The data were fit to the function $F(\omega) = R\left[n(\omega)+1\right] \mathrm{Im}\chi(\omega)$, where $\chi(\omega)$ is the complex susceptibility of two damped harmonic oscillators which are coupled together.

The imaginary part of the complex susceptibility can be compactly expressed[26] in terms of the two mode coupling Green's function $G_{ij}(\omega)$ and the mode strengths P_i, P_j as

$$\mathrm{Im} \quad (\omega) = \mathrm{Im} \sum_{ij} P_i P_j G_{ij}(\omega) \quad .$$

The terms $G_{ij}(\omega)$ can be determined from the coupled mode equation

$$\begin{bmatrix} (\omega_a^2 - \omega^2 + i\omega\Gamma_a) & \Delta^2 \\ \Delta^2 & (\omega_b^2 - \omega^2 + i\omega\Gamma_b) \end{bmatrix} \begin{bmatrix} G_{11} & G_{12} \\ G_{21} & G_{22} \end{bmatrix} = \begin{bmatrix} 1 & 0 \\ 0 & 1 \end{bmatrix}$$

The solution to this equation gives the following expression

$$G_{11} = \frac{\omega_b^2 - \omega^2 + i\omega\Gamma_b}{(\omega_a^2 - \omega^2 + i\omega\Gamma_a)(\omega_b^2 - \omega^2 + i\omega\Gamma_b) - \Delta^4}$$

$$G_{22} = \frac{\omega_a^2 - \omega^2 + i\omega\Gamma_a}{(\omega_a^2 - \omega^2 + i\omega\Gamma_a)(\omega_b^2 - \omega^2 + i\omega\Gamma_b) - \Delta^4}$$

and $$G_{12} = G_{21} = \frac{-\Delta^2}{(\omega_a^2 - \omega^2 + i\omega\Gamma_a)(\omega_b^2 - \omega^2 + i\omega\Gamma_b) - \Delta^4} .$$

There are seven adjustable parameters involved in the fit of the Raman spectrum to this function. They are R, P_b/P_a, ω_a, ω_b, Γ_a/ω_a^2, Γ_b, Δ. R is a normalization constant and P_b/P_a indicates the strength ratio of the optic mode to the overdamped mode. $\Gamma_a/\omega_a^2 = \tau$ and Γ_b are respectively the Debye relaxation time of the overdamped mode and the width of the optic mode. Δ is the coupling parameter between the overdamped and optic modes and has the dimensions of inverse time.

Computation

$F(\omega)$ is a complicated function and it was my experience that the initial guesses of parameters needed to be quite accurate for the

program to converge on the observed data points. Part of the problem in the fit is with the coupling constant parameter Δ. This appears in the equations in the forms Δ^2 and Δ^4. Apparently some of the early workers in the coupled mode problem ignored the terms involving Δ^4. This greatly simplifies the resulting function. The values obtained for Δ in the cases of ADP and KDP do not justify dropping the Δ^4 term which is comparable or larger than $\omega_a^2 \omega_b^2$. Therefore, if Δ^4 is dropped, the resulting model function no longer corresponds to the coupled harmonic oscillator problem.

Numerically, the effect of the Δ^4 term can be seen in Figure 6. Figure 6 shows the computer fit to the B_2 mode of ADP at 147° K by neglecting the Δ^4 term. The bottom plot in the same figure is the exact function $F(\omega)$ using the fitted parameters obtained. Even though the fit in Figure 6 is good the parameters obtained by neglecting the Δ^4 term are clearly unacceptable for the exact function $F(\omega)$. By keeping the Δ^4 term in the fit program, a different set of parameters may be obtained, and the two sets of data are compared in Table II. The quality of fit numerically is about the same in the two cases, but only the parameters fit to the exact expression (i.e., keeping the Δ^4 terms) are meaningful on physical grounds.

When the Δ^4 terms are kept, the program is very sensitive to the initial guesses of parameters. One way to come up with a set of initial guesses is to use the parameters obtained in a least-squares fit by neglecting the Δ^4 term. One then obtains new sets of parameters by gradually turning on the strength of the Δ^4 term. This

Figure 6. The top graph shows the quality of fit which can be achieved in the coupled mode problem when Δ^4 term is ignored. Dots are data points and the crosses are calculated points.

The bottom graph shows the result of using the parameters obtained above in the exact coupled mode equation where the Δ^4 term has been retained.

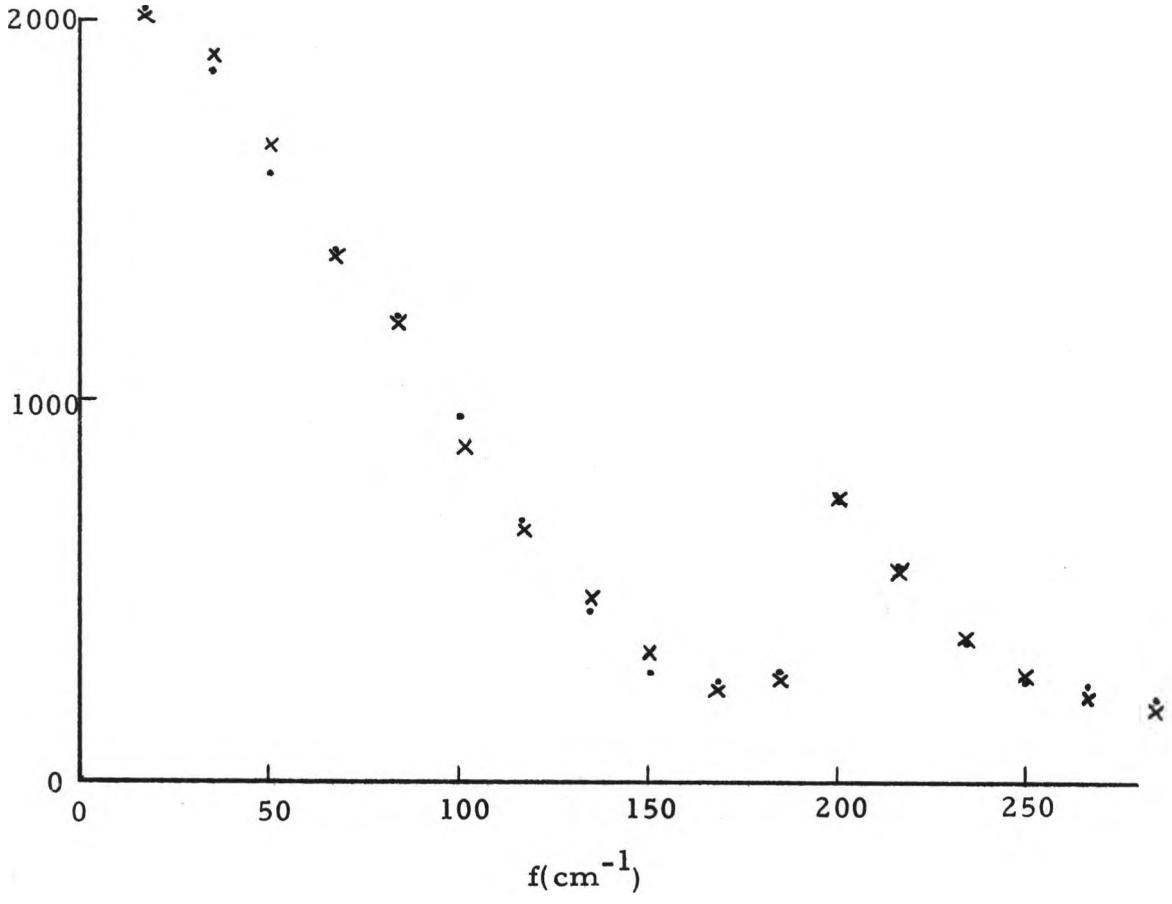
2000
1000
0
0
50
100
150
200
250
f(cm-1)

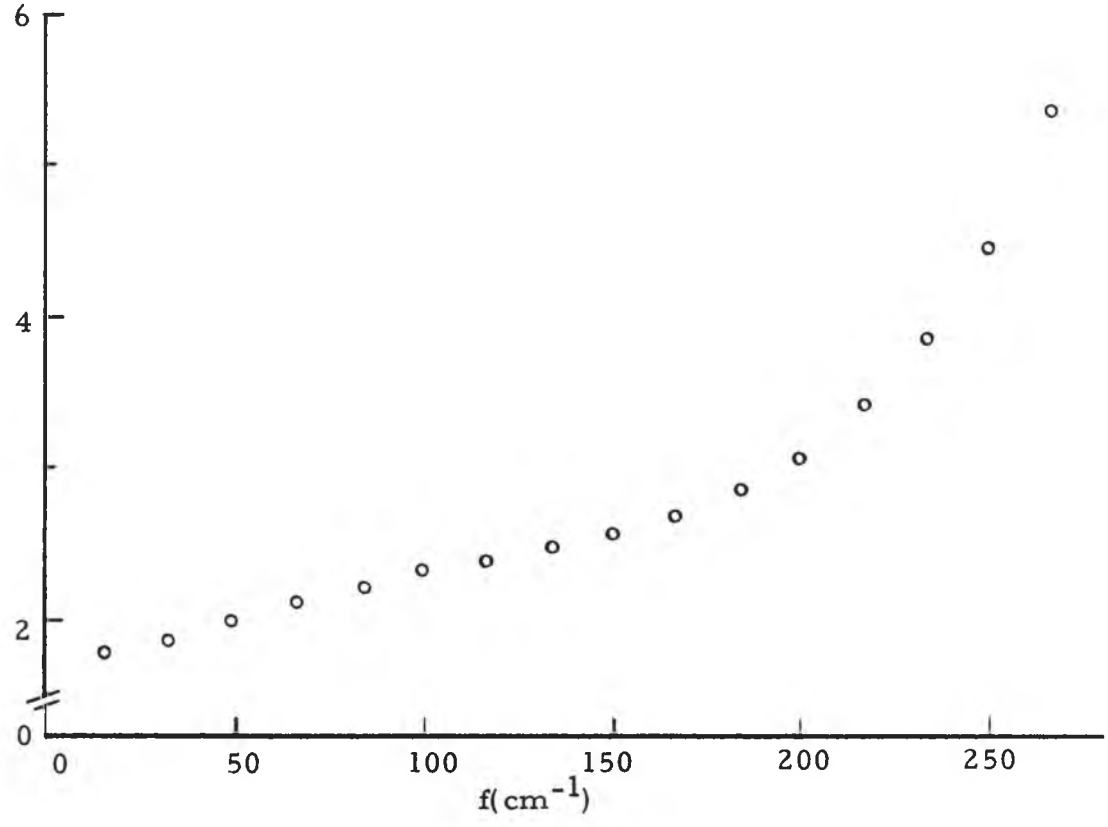
6
4
2
0
0
50
100
150
200
250
f(cm-1)

Table 2. Comparison of lease squares fit parameters obtained including Δ^4 (in top row) and neglecting it (in bottom row) in the coupled mode problem. The sample is ADP at about 147°. Parameter values for ω_a, ω_a^2/Γ, ω_b, Γ and Δ can be converted to cm^{-1} by multiplying by 5/3.

R	P_b/P_a	ω_a	Γ_a/ω_a^2	ω_b	Γ_b	Δ
$(-6.06 \pm .5)\times10^6$	$0.248 \pm .005$	$78.7 \pm .5$	$0.0215 \pm .0005$	$117.8 \pm .5$	$9.89 \pm .5$	$66.9 \pm .5$
$(-1.37 \pm .5)\times10^6$	$0.0206 \pm .0005$	$68.3 \pm .5$	$0.0298 \pm .0005$	$117.6 \pm .5$	$17.3 \pm .5$	$270. \pm .5$

way an acceptable set of initial guesses of the parameter may be derived and used for the exact function.

The fact that the Δ^4 terms must be kept means the optic and overdamped modes are strongly coupled, i.e., the values of Δ, ω_a and ω_b are comparable. The result of our analysis of the B_2 modes of KDP and ADP for temperatures above the phase transition are summarized in Table III. It is interesting to note that the value for Δ is reasonably temperature independent.

KDP Results

The analysis of the coupled B_2 mode of KDP for temperatures approaching the phase transition from above yields plots of $1/\chi(0)$, ω_a^2 and T/τ as a function of temperature as shown in Figure 7. Like the original work of Kaminow and Damen, we plot $1/\chi(0)$ in arbitrary units. The striking feature of the plots in Figure 7 is that all quantities $1/\chi(0)$, ω_a^2 and T/τ vary linearly in temperature as $(T-T_c')$, with different values of T_c' for each quantity plotted. The static susceptibility associated with the coupled modes can be easily derived from the Green's Function expression presented earlier. The result is

$$\frac{\chi(0)}{P_a^2} = \frac{\left[\omega_b^2 + \left(\frac{P_b}{P_a}\right)\omega_a^2 - 2\left(\frac{P_b}{P_a}\right)\Delta^2\right]}{(\omega_a^2\omega_b^2 - \Delta^4)}$$

where again the a subscript refers to the overdamped mode.

Table 3. Parameters derived from the least squares fitting program as a function of temperature for ADP and KDP. The parameter values for ω_a, ω_a^2/Γ_a; ω_b, Γ_b and Δ can be converted to cm^{-1} by multiplying the listed number by 5/3.

ADP B_2							
Temp.	P(1) = R	P(2)=P_b/P_a	P(3) = ω_a	P(4)=Γ_a/ω_a^2	P(5) = ω_b	P(6) = Γ_b	P(7) = Δ
229°K	$(-6.1\pm5)\times10^6$	$0.200\pm.005$	$90.2\pm.5$	$.0175\pm.0005$	$113.5\pm.5$	$13.2\pm.5$	$71.3\pm.5$
198°	-6.23×10^6	0.220	85.0	.0185	115.5	12.1	69.4
173°	-5.37×10^6	0.228	82.0	.1094	116.1	10.4	68.4
166°	-5.37×10^6	0.240	80.1	.0201	116.8	10.4	67.6
162.5°	-5.52×10^6	0.235	81.3	.0199	115.8	10.3	68.6
156°	-5.58×10^6	0.240	79.8	.0208	116.9	10.4	67.5
154°	-5.60×10^6	0.242	79.8	.0207	117.4	9.70	67.6
152°	-5.25×10^6	0.255	77.3	.0211	117.7	9.66	65.9
151°	-5.55×10^6	0.246	80.2	.0215	117.5	10.2	67.0
149.8°	-6.02×10^6	0.246	78.7	.0215	117.4	10.00	66.5
149.4°	-6.09×10^6	0.245	79.2	.0212	117.5	9.98	67.4
147.9°	-6.06×10^6	0.239	79.2	.0219	117.0	9.63	66.9
147°	-6.06×10^6	0.248	78.7	.0215	117.8	9.89	66.9
KDP B_2							
292.5°	$(-7.07\pm.5)\times10^6$	$.0596\pm.005$	$79.4\pm.5$	$.0252\pm.0005$	$94.0\pm.5$	$4.63\pm.5$	$67.3\pm.5$
244°	-7.18×10^6	.0525	73.4	.0255	94.8	3.88	68.8

Table 3. (Continued)

Temp.	P(1) = R	P(2)=P_b/P_a	P(3) = ω_a	P(4)=Γ_a/ω_a^2	P(5) = ω_b	P(6) = Γ_b	P(7) = Δ
154	-7.78×10^6	.0935	54.7	.0341	100.9	2.82	68.6
151	-7.74×10^6	.0906	54.5	.0346	100.6	2.77	68.8
147	-8.84×10^6	.104	53.0	.0368	101.6	4.02	68.9
141	-8.06×10^6	.0999	52.0	.0368	101.4	3.19	68.6
133	-8.07×10^6	.105	49.9	.0397	102.3	3.14	68.6
128	-8.17×10^6	.109	49.1	.0418	102.4	3.22	68.8
124	-8.05×10^6	.129	47.9	.0453	103.4	3.79	68.0

Figure 7. KDP graphs of the inverse static dielectric susceptibility $1/\chi(0)$ (actually $P_a^2/\chi(0)$ is plotted), the square of the overdamped mode frequency, ω_a^2 and the temperature-weighted reciprocal Debye relaxation time $T/\tau = T\omega_a^2/\Gamma_a$ for the overdamped mode.

$1/\chi(0)$ [arbitrary units]; ω_a^2 [10^4 (cm^{-1})^2]
0
0.5
1.0
1.5
2.0
T [°K]
0
50
100
150
200
250
T/τ [10^{14} °K/sec]
2
4
6
8
T/τ
ω_a^2
$1/\chi(0)$

The transition temperature obtained from the $1/\chi(0)$ plot yields $T_c = 116°K$ in good agreement with result of Kaminow and Damen,[8] and Wilson and Cummins[21] to within the accuracy of my temperature measurement ($\pm 1°K$).

The effect of the proton-phonon coupling produces a linear temperature dependence on the soft (overdamped) mode frequency, ω_a^2. Displacive ferroelectrics show similar behavior.[1,22] This is contrary to the conclusions of previous experimenters. They (Kaminow, et. al., and Wilson, et. al.) have ignored the proton-phonon coupling. The inferred transition temperature from the ω_a^2 plot is $T_c' = 30°K$.

The temperature dependence of T/τ is again linear which is different from that given by Kaminow and Damen. This linear dependence is expected because $\omega_a^2 \alpha (T-T_c')$ and $\Gamma_a \alpha T$ in the anharmonic oscillator approximation. The inferred transition temperature is yet different, $T_c'' = 70°K$.

The fact that the transition temperatures extrapolated from various dynamical parameters are different from the true transition temperature (122°K for KDP) is not entirely unreasonable. It is not an uncommon situation: the extrapolated temperatures have been different from the true T_c by about 40°K in $PbTiO_3$ and about 70°K in CsH_2AsO_4. One way to account for this anomalous behavior is to treat the short lifetime of the soft-mode excitations as suggested by Cowley, et. al.[27]

The data for the coupled E mode, and the B_2 mode below the transition in KDP are not analyzed here. Due to the extreme overdamping in these cases, the data may be fitted to a simpler model due originally to Breit and Wigner.[28] Scott[29] has recently analyzed these spectra.

ADP Results

In analogy with anti-ferromagnetism,[30] the critical mode responsible for the transition from above is the zone-boundary mode. Raman data which probes the zone-center mode gives complimentary information about the transition. The "soft mode" below the phase transition may be probed by light scattering. Unfortunately the ADP crystal shatters below the transition temperature which makes the usual experiment impossible.

The parameters $1/\chi(0)$, ω_a^2, and T/τ obtained from the analysis of the B_2 mode of ADP as a function of temperature are plotted in Figure 8. Again, a straight line can be drawn for each plot with good accuracy. We do not extrapolate T_c's for $1/\chi(0)$ and ω_a^2, because the zone-center phonons in the high-temperature phase do not necessarily give direct information of the phase transition in an anti-ferroelectric. A transition temperature is extrapolated from the T/τ plot, however for comparison.

Ryan[23] et. al., reported only T/τ plots. Besides possible disagreement on temperature measurements, the extrapolated

Figure 8. ADP graphs of the inverse static dielectric susceptibility $1/\chi(0)$ (actually $P_a^2/\chi(0)$ is plotted), the square of the overdamped mode frequency, ω_a^2 and the temperature-weighted reciprocal Debye relaxation time $T/\tau = T\,\omega_a^2/\Gamma_a$ for the overdamped mode.

1/χ(0) [arbitrary units] ; T/τ [10^14 °K/sec]
0
1
2
3
4
5
6
7
T(°K)
0
50
100
150
200
250
ω_a^2 [10^4 (cm^-1)^2]
0
1
2
1/χ(0)
T/τ
ω_a^2

temperature in this report is 58° K in contrast to their value of 29° K. It is seen that a straight line can be drawn accurately for T/τ in Figure 8. The scatter of the only five data points in Ryan, et. al., makes the reliability of their straight line questionable.

The temperature measurements in this research have been carefully made. The temperatures at different positions in the crystal were measured and a variation of about 2° K was found between the extremes. A thermocouple situated about 3 mm away from the scattering volume measured the temperature of the scattering volume within $\pm$ 1° C. A sequence of the E spectra of ADP at different temperatures is shown in Figure 9. Comparing these to the corresponding spectra of Ryan, et. al., one would conclude that their reported temperature values were perhaps lower than the true temperature of the scattering volume of their sample, or that their resolution was poorer than reported.

The coupling of protons and optical phonons in the E spectra, although more complex, can be analyzed as well. Such analyses are in progress, but the results will not be reported here.

Figure 9. ADP E mode [y(xz)x] spectra at several temperatures. Resolution is 4 cm^{-1} at 4880 A.

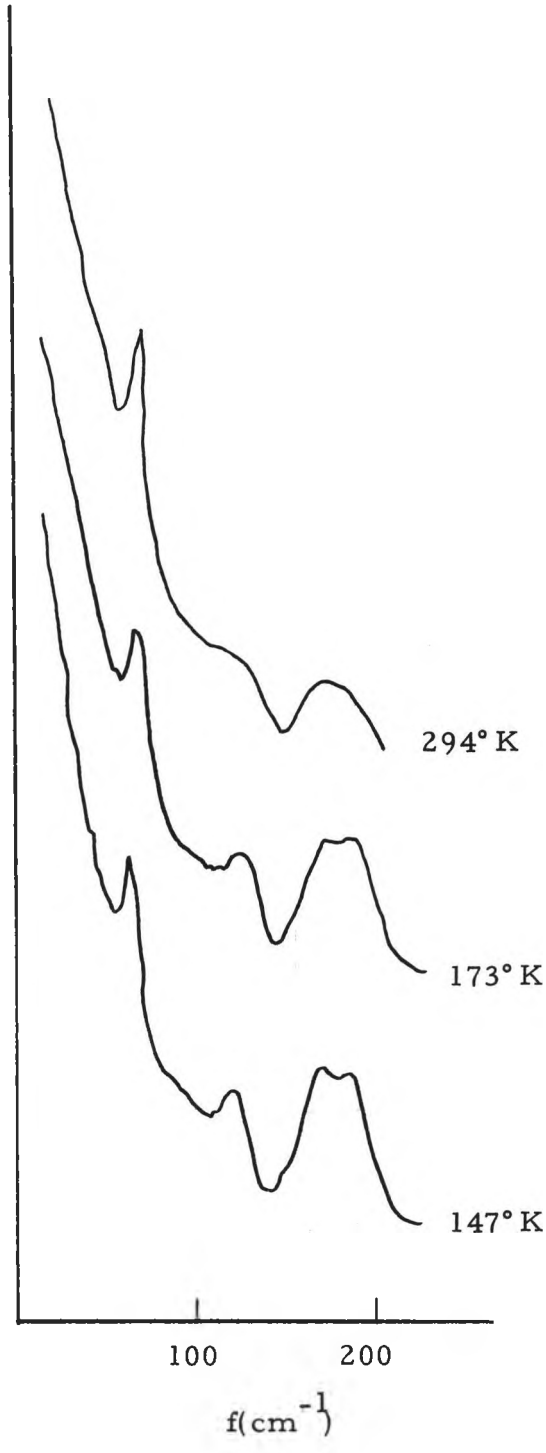
294° K
173° K
147° K
100
200
f(cm^{-1})

CHAPTER IV

CONCLUSIONS

Clearly, several of the questions posed in Chapter I of this dissertation have been answered in the course of the research presented here. Five of the six Raman active optical lattice modes predicted by group theory have been positively identified in both ADP and KDP. In addition, interesting observations have been made of the splitting of the $(PO_4)^{3-}$ ion modes under the local crystalline field of S_4 symmetry in these crystals.

The broad modes associated with polarization fluctuations in ADP have indeed been observed in both the B_2 and E spectra. Furthermore, the need to consider the coupling between the B_2 proton tunneling mode and the optical lattice mode of the same symmetry has been confirmed in both ADP and KDP. In fact, the strength of the proton-optical-phonon coupling was found to be comparable to the phonon frequencies and could not be considered as a perturbation on the two oscillator systems.

The results for the overdamped mode in KDP behave as though the crystal is a displacive ferroelectric, showing the linear temperature dependence of the square of the frequency ω_a. The quantities T/τ and $1/\chi(0)$ also vary linearly in temperature as expected. The extrapolated

transition temperature from each of these parameters ω_a^2, T/τ and $1/\chi(0)$, is different. This is a similar result as observed in CsH_2AsO_4. A similar analysis was carried out in ADP and the results while in qualitative agreement with other researchers, represented an improvement in reliability.

Several aspects of the Raman spectra obtained for ADP and KDP warrant further investigation. The extent to which coupling occurs between the E species tunneling mode and the lattice modes of that symmetry needs to be determined. This study is presently in progress. ADP shatters when passing through the phase transition but Raman studies below the transition could still be carried out by utilizing powdered sample techniques.

The line shape anomalies mentioned in Chapter I are presently under investigation by other members of our quantum electronics research group.

REFERENCES

1. W. Cochran, Advan. Phys. 9, 387 (1960) and 10, 401 (1961).

2. J. M. Worlock, J. F. Scott and P. A. Fleury, in Light Scattering Spectra of Solids, edited by G. B. Wright (Springer, New York, 1969).

3. J. C. Slater, J. Chem. Phys. 9, 16 (1941).

4. R. Blinc, J. Phys. Chem. Solids, 13, 204 (1960).

5. P. G. de Gennes, Solid State Commun., 1, 132 (1963).

6. M. Tokunaga and T. Matsubara, Prog. Theor. Phys. 35, 581 (1966); M. Tokunaga, Prog. Theo. Phys. 36, 857 (1966).

7. F. Jona and G. Shirane, Ferroelectric Crystals (Pergamon Press, 1962).

8. I. P. Kaminow and T. C. Damen, Phys. Rev. Letters, 20, 1105 (1968).

9. K. K. Kobayashi, J. Phys. Soc. Jap., 24, 497 (1968).

10. I. P. Kaminow, Phys. Rev., 138, 1539 (1965).

11. R. K. Khanna and C. W. Reimann, Spectra-Physics Raman Tech. Bull., No. 3, 1970 (Unpublished).

12. W. G. Fateley, N. T. McDevitt and F. F. Bentley, Appl. Spectry. 25, 155 (1971).

13. C. Y. She, T. W. Broberg and David F. Edwards, Phys. Rev. B 4, 1580 (1971).

14. G. L. Paul and H. Montgomery, "Symmetry of Atonic Vibrations in KH_2PO_4. (Preprint, Submitted to Proc. Roy. Soc. Edinburgh).

15. J. P. Coignac and H. Poulet, J. De Phys. 32, 679, (1971).

16. E. A. Popova and A. I. Stekanov, Fiz. Tverd. Tela. 12, 51 (1970). [Sov. Phys. Solid State, 12, 40 (1970).]

17. G. Herzberg, Infrared and Raman Spectra of Polyatomic Molecules (Van Nostrand, Princeton, N. J., 1945).

18. J. R. Durig and D. J. Antion, J. Chem. Phys., 51, 3639 (1969).

19. E. Wiener, S. Levin and I. Pelah, J. Chem. Phys., 52, 2881 (1970).

20. R. Wychoff, Crystal Structures, 2nd Ed. (Interscience, New York, 1963), Vol. III.

21. C. M. Wilson and H. Z. Cummins, "Raman Scattering in KH_2PO_4," (to be published, Proc. 2nd International Light Scattering Conference, Paris, 1971).

22. C. M. Wilson, Ph.D. Thesis, The Johns Hopkins Univ., (1970).

23. J. F. Ryan, R. S. Katiyar and W. Taylor, "Raman Scattering from Ferroelectric Modes in KDP Isomorphous Phosphates and Arsenates", (Submitted for publication to J. of Phys. C).

24. "Regression Analysis Determination of Nonlinear Parameters", (Stat 31 R, Statistics Library, Colo. State Univ. Fort Collins, Colo.).

25. H. B. Callen, in Fluctuation Relaxation and Resonance in Magnetic Systems, edited by D. Ter Haar (Oliver and Boyd, Edinburgh and London, 1962).

26. R. S. Katiyar, J. F. Ryan and J. F. Scott, Phys. Rev. B4, 2635 (1971).

27. R. A. Cowley, G. J. Coombs, R. S. Katiyar, J. F. Ryan and J. F. Scott, J. Phys., C 4, L203 (1971).

28. G. Breit and E. Wigner, Phys. Rev. 49, 519 (1936).

29. J. F. Scott and C. M. Wilson, "Proton-Phonon Interactions in KDP", Solid State Commun. (to be published).

30. W. Marshall and R. D. Lowde, Rept. Prog. Phys. 31, 705 (1968).

31. Y. D. Harker, Jon D. Masso and David F. Edwards, J. Chem. Phys. 50, 5420 (1968).

32. Jon D. Masso, C. Y. She and David F. Edwards, Phys. Rev. B 1, 4179 (1970).

33. D. Des Cloizeaux, in Theory of Condensed Matter (International Atomic Energy Agency, Vienna, 1968).

APPENDIX I

ADP-KDP STRUCTURE

Discussions of the structure of crystals ADP and KDP must be broken into the temperature region above the phase transition and the temperature region below it.

KDP Above the Transition Temperature

The crystal KDP in its paraelectric phase can be considered as consisting of K^+ and $(H_2PO_4)^-$ ions as its elementary constituents. There are two K^+ ions and two $(H_2PO_4)^-$ ions per primitive unit cell. The crystal is of the body center tetragonal structure as is easily seen in Figure 1. The solid circles which denote $(H_2PO_4)^-$ ions can be considered to locate a phosphorus ion P^{5+} which is tetrahedrally surrounded by the four oxygens. If one of these phosphorus ions is located at the origin, then another one is located at $(0, \frac{1}{2}, \frac{1}{4})$ in an (x, y, z) system of coordinates. These two phosphorus ions are not equivalent. The nearest neighbor equivalent phosphorus to the one at (0, 0, 0) being located at $(\frac{1}{2}, \frac{1}{2}, \frac{1}{2})$, $(-\frac{1}{2}, \frac{1}{2}, \frac{1}{2})$ and $(-\frac{1}{2}, -\frac{1}{2}, \frac{1}{2})$.

Some details of the hydrogen bonding in ADP and KDP are important in my research. It can be seen in Figure 1 that the KDP and ADP crystals can be viewed as having two interlaced body centered lattices of $(PO_4)^{3-}$ tetrahedra. One is located at $(0, \frac{1}{2}, \frac{1}{4})$

relative to the other. The hydrogen bonds are oriented nearly parallel to the x or y crystallographic direction and therefore nearly perpendicular to the c-axis. Each hydrogen bonds an oxygen at the top of one tetrahedron to an oxygen at the bottom of a tetrahedron in the other sublattice (Figure 10).

The vibrational modes in this crystal consist of three distinct types. Lattice modes due to the relative motion of the K^+ and PO_4^{3-} ions is one type. The internal vibrations of the PO_4^{3-} complex is another and the motion of the hydrogen ions along their bond direction is yet another. Neutron diffraction studies have detect the elogation of changes in one dimension near the hydrogen position. This could be due to either a centrally located hydrogen ion undergoing anisotropic motion or to two half-hydrogens moving in a double minimum potential between the two oxygen ions. The double well potential associated with the two half-hydrogens is presently the popular model for the hydrogen bond in KDP.

KDP Below the Transition Temperature

At temperatures below about 122°K KDP has orthorhombic structure with the unit cell symmetry corresponding to the C_{2V}^{19} point group.[20] In this state the crystal is ferroelectric with the P^{5+} ions being shifted slightly parallel to the c direction of the original tetragonal structure. A related feature is that the hydrogen ions are now collectively ordered in the potential well nearest to the lower (or higher) oxygens in the PO_4^{3-} tetrahedra.

Figure 10. Projection of the $(PO_4)^{3-}$ sublattices on the (0, 0, 1) plane. Dotted lines represent hydrogen bonds. Subscripts correlate to the inequivalent sites at Figure 1.

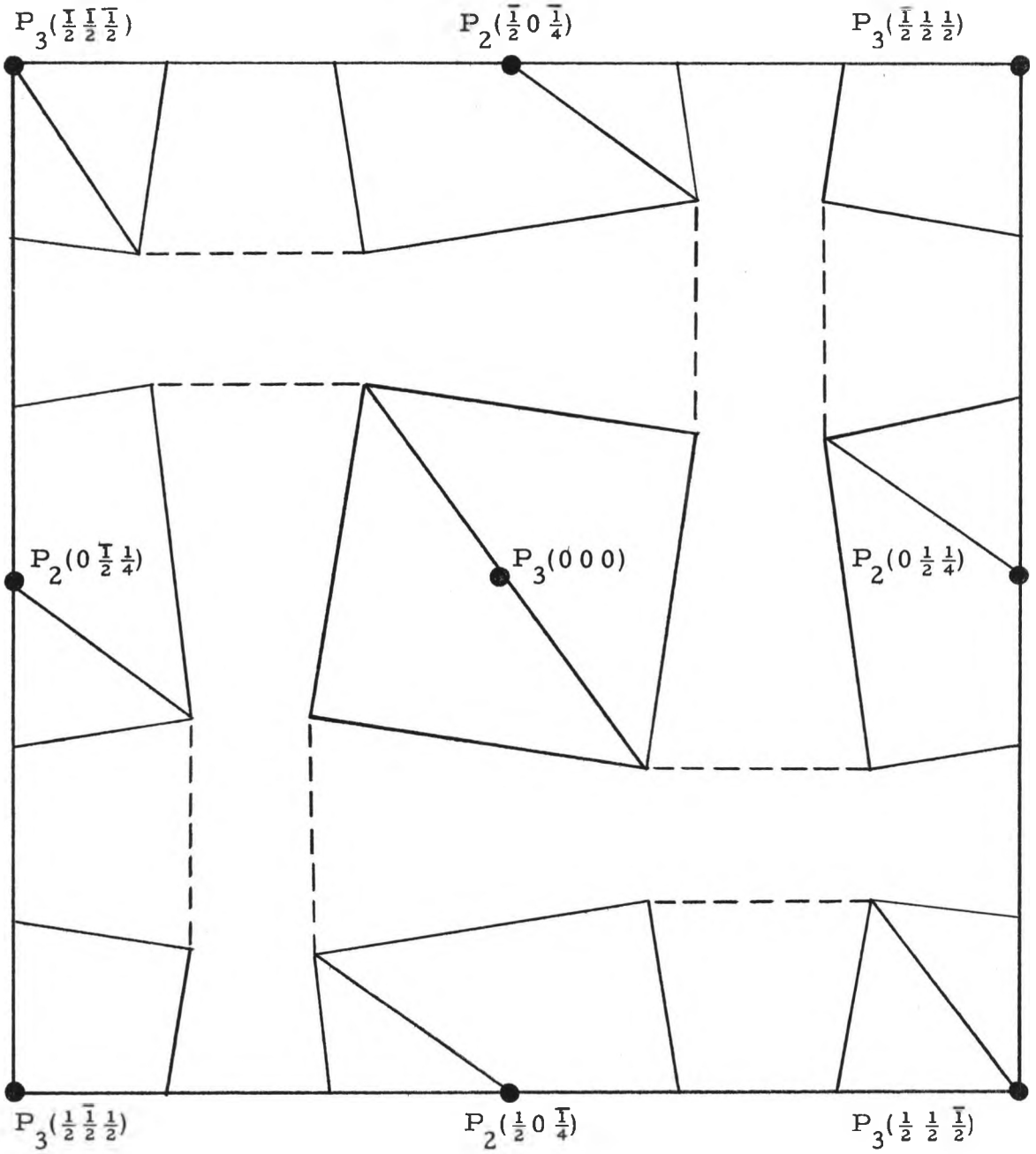
$P_3(\bar{\frac{1}{2}}\,\bar{\frac{1}{2}}\,\bar{\frac{1}{2}})$
$P_2(\bar{\frac{1}{2}}\,0\,\bar{\frac{1}{4}})$
$P_3(\bar{\frac{1}{2}}\,\frac{1}{2}\,\frac{1}{2})$
$P_2(0\,\bar{\frac{1}{2}}\,\frac{1}{4})$
$P_3(0\,0\,0)$
$P_2(0\,\frac{1}{2}\,\frac{1}{4})$
$P_3(\frac{1}{2}\,\bar{\frac{1}{2}}\,\frac{1}{2})$
$P_2(\frac{1}{2}\,0\,\bar{\frac{1}{4}})$
$P_3(\frac{1}{2}\,\frac{1}{2}\,\bar{\frac{1}{2}})$

ADP Above the Transition Temperature

Above about 147°K ADP is paraelectric and has the same basic structure as paraelectric KDP. The sites of K^+ ions in KDP designate the positions of the NH_4^+ ions in ADP. Also, the dimensions of the unit cell are given by a = 7.510 Å and c = 7.564 Å. In other respects the paraelectric ADP and KDP are structurally the same.

ADP Below the Transition Temperature

Below the phase transition ADP is antiferroelectric and belongs to the D_2^4 space group.[20] Since the ADP crystal shatters below the phase transition, there has been little interest in this phase to date.

APPENDIX II

RAMAN SCATTERING

Descriptive

If a beam of monochromatic light is shone into a transparent substance, scattered light can be observed emanating from the illuminated path. Typically, most of this scattered light is due to impurity scattering (Raleigh Scattering) in which case the scattered light has the same frequency as the incident light or it is resonantly absorbed and reemitted at a frequency equal to or lower than the incident frequency (fluorescence). There is an additional and intriguing contribution to the spectrum of scattered light, however. A small fraction of the incident light is inelastically scattered from the sample in such a way that it shows up as sidebands symmetrically displaced on the high and low frequency sides of the incident frequency. The symmetrical displacement of the sidebands in frequency implies symmetrical displacement in energy. The energy shifts correspond to characteristic energies within the sample. That is, the incident radiation interacts with the sample in such a way as to be scattered with components some of which are shifted up and others which are shifted down by frequencies characteristic of the substance. This is usually referred to as Raman scattering. The low

frequency component is referred to as Stokes radiation, while frequencies elevated from the incident frequency are referred to as antistokes.

In some cases normal mode vibrations within the sample are responsible for the Raman shifted spectrum. The energy shifts can then be related to the spring constants associated with the bond involved in the vibration, i.e.,

$$\omega^2 = \frac{\kappa}{m^*}$$

where ω = vibrational frequency = Raman shift, κ is the spring constant and m^* is the effective mass associated with that vibrational motion.

Not all normal mode vibrations can give rise to a Raman shift, however. Certain symmetry requirements must be met if a particular mode is to be Raman active (give rise to a Raman shift).

If we consider an induced dipole moment in a crystal, we can write

$$m_i = \alpha_{ij} E_j \tag{1}$$

where P_i is the electric dipole moment per unit volume, α_{ij} is a general element of the polarizability tensor for the crystal and E_j is the applied electric field. If the applied electric field is due to the incident light and therefore at optical frequencies, we can consider

α_{ij} to be composed of two parts, namely:

$$\alpha_{ij} = \alpha_{ij}\,(\text{ionic}) + \alpha_{ij}\,(\text{electronic}) \tag{2}$$

where α_{ij} (ionic) is the polarizability due directly to the displacement of the ion cores in the lattice induced by the applied electric field $\vec{E}$. The α_{ij} (electronic) component is due to the displacement of the electron cloud by this same electric field $\vec{E}$. The masses involved in the ion cores prevents them from following the optical frequency electric field. The electrons, however, can follow the optical frequency field. For this reason I will consider only the electronic contribution to the polarizability tensor in the remainder of this thesis. I will also drop the (electronic) label.

In general, the electronic polarizability of a crystal will be a function of the normal mode coordinates q_ℓ. If α_{ij} is expanded as a function of q_ℓ, we have

$$\alpha_{ij} = (\alpha_{ij})_{q_\ell=0} + \left(\frac{\partial \alpha_{ij}}{\partial q_\ell}\right)_{q_\ell=0} q_\ell + \left(\frac{\partial^2 \alpha_{ij}}{\partial q_m \partial q_\ell}\right)_{q_\ell=0,\ q_m=0} q_\ell q_m + \ldots . \tag{3}$$

where the summation convention is implied by the repeated index. I will consider the first two terms. Substituting equation (3) into equation (1) we have

$$(4) \qquad m_i = \left[(\alpha_{ij})_{q_\ell = 0} + \left(\frac{\partial \alpha_{ij}}{\partial q_\ell} \right)_{\substack{q_\ell \\ q_\ell = 0}} \right] E_j$$

$$= \frac{1}{2} \left[(\alpha_{ij})_{q_\ell = 0} + \frac{1}{2} \left(\frac{\partial \alpha_{ij}}{\partial q_\ell} \right)_{q_\ell = 0} (q_\ell^+ \; e^{i\omega_\ell t} + q_\ell^- e^{-i\omega_\ell t}) \right]$$

$$\left[E_j^+ e^{i\omega t} + E_j^- e^{-i\omega t} \right]$$

where the time dependence of the phonon coordinates and electric field have been included in terms of ω_ℓ and ω, respectively. The $(\alpha_{ij})_{q_\ell = 0}$ term gives rise to scattering only at the frequency ω of the incident light. The $\left(\frac{\partial \alpha_{ij}}{\partial q_\ell} \right)_{q_\ell = 0}$ term is the source of Raman shifted radiation, as it produces sum $(\omega + \omega_\ell)$ and difference $(\omega - \omega_\ell)$ frequencies in the resulting product. The Raman Effect is then seen to depend upon a non-zero first order change in the electronic polarizability with respect to the phonon coordinates.

The Raman radiated energy per unit solid angle per unit time due to $\left(\frac{\partial \alpha_{ij}}{\partial q_\ell} \right)_{q_\ell = 0}$ is[22]

$$F_{ij}(\omega, \Delta\omega) = A\omega^4 \left| \left(\frac{\partial \alpha_{ij}}{\partial q_\ell} \right)_{q_\ell = 0} E_0 \right|^2 Q(\Delta\omega)$$

using the fluctuation-dissipation theorem,[22,23]

$$= A\omega^4 \left| \left(\frac{\partial \alpha_{ij}}{\partial q_\ell} \right)_{q_\ell = 0} E_0 \right|^2 \left[n(\Delta\omega) + 1 \right] \chi''(\Delta\omega).$$

The quantity A is a constant, E_0 is the amplitude of the incident electric field, $Q(\Delta\omega)$ is the power spectral density of the fluctuations

in phonon coordinates, $n(\Delta\omega)$ is the Bose factor and $\chi''(\omega, \omega_\ell)$ is the imaginary part of the dielectric susceptibility associated with the phonon mode, ℓ.

Experimental

The Raman Spectra were taken with the apparatus schematically represented in Figure 11. Sample illumination was accomplished with an Argon Ion laser operated at 0.5 Watts at a wavelength of 4880 Å. This laser has a self stabilizing feature and internal power meter. On a 0.5 Watt = half Scale reading, no power fluctuation could be observed in the laser output. The incident polarization could be controlled by means of a polarization rotor built into the laser framework. Incident light was focused into the sample with a 62 millimeter focal length lense. Scattered light was collected by a 10 cm focal length lense which was aperatured down to f/d. The scattered light next passed through a polarization analyzer which defined the polarization to be allowed into the spectrometer. Before entering the spectrometer, the polarization was scrambled to eliminate the polarization dependence of the transmission of the spectrometer. A one meter Czerny-Turner double spectrometer was operated with slit widths corresponding to about four wavenumbers (cm^{-1}) resolution at 4880 Å.

The scattered signal was detected with a photomultiplier tube with an S-20 response. This tube was cooled to 0° Centigrade at

Figure 11. Schematic of the Raman experimental system.

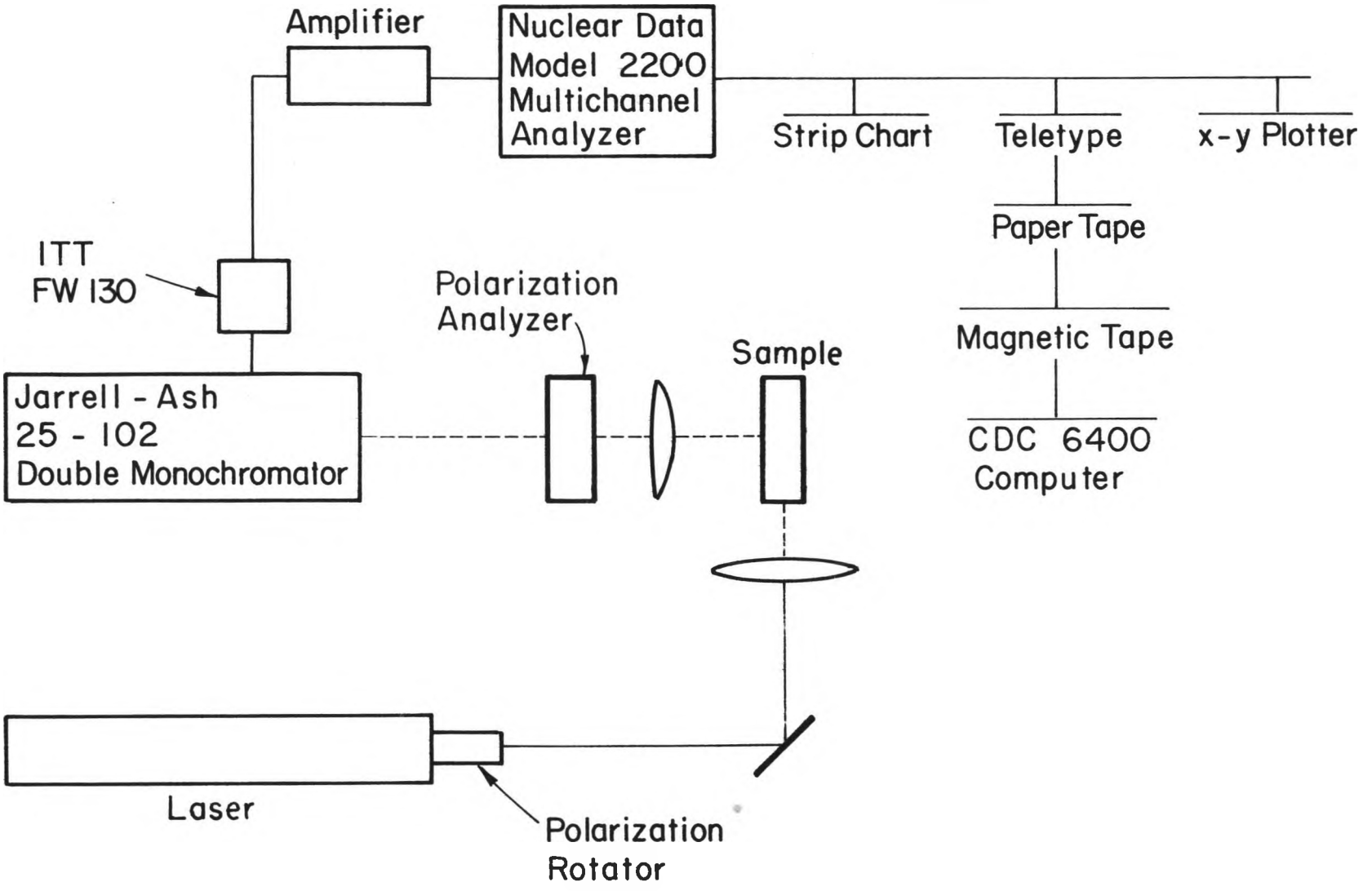
Amplifier
Nuclear Data
Model 2200
Multichannel
Analyzer
Strip Chart
Teletype
x-y Plotter
Paper Tape
Magnetic Tape
CDC 6400
Computer
ITT
FW 130
Polarization
Analyzer
Sample
Jarrell - Ash
25 - 102
Double Monochromator
Laser
Polarization
Rotator

which approximately four dark counts per second were observed. The signal from the photomultiplier tube was amplified and photon counting techniques were then applied.[31,32] The spectrometer was advanced through the spectrum continuously while the multichannel analyzer was advanced in through the channels in steps. The multichannel analyzer dwell time varied from two to eight sec. per channel depending upon the available scattered signal and the drive speed of the spectrometer.

Temperature dependent studies were carried out using a Cyro-Tip refrigerator which utilizes the Joule-Thompson effect in cooling. The gas used in the refrigeration cycle for these studies was nitrogen. Thermal contact between the sample and the cold finger of the regrigerator was accomplished using Dow Corning 200 fluid. The temperature was monitored with Cooper-Constantan thermocouples attached simultaneously to the sample and the cold finger. The resulting spectrum was then typically recorded with an x-y plotter and punched on paper tape. The temperature dependent data were then fit using least squares fitting program[24] and relevant parameters extracted.

Typed and Reproduced by
TYPE-INK Fort Collins